DEVELOPMENT AND CHARACTERIZATION OF TIN BASED ANODE MATERIALS FOR LI-ION BATTERIES

A THESIS SUBMITTED TO
THE GRADUATE SCHOOL OF NATURAL AND APPLIED SCIENCES
OF
MIDDLE EAST TECHNICAL UNIVERSITY

BY

EMRE YILMAZ

IN PARTIAL FULFILLMENT OF THE REQUIREMENTS
FOR
THE DEGREE OF MASTER OF SCIENCE
IN
METALLURGICAL AND MATERIALS ENGINEERING

FEBRUARY 2018

Approval of the thesis:

DEVELOPMENT AND CHARACTERIZATION OF TIN BASED ANODE MATERIALS FOR LI-ION BATTERIES

submitted by **EMRE YILMAZ** in partial fulfillment of the requirements for the degree of **Master of Science in Metallurgical and Materials Engineering Department, Middle East Technical University** by,

Prof. Dr. G. Dural Ünver _____
Dean, Graduate School of **Natural and Applied Sciences**

Prof. Dr. C. Hakan Gür _____
Head of Department, **Metallurgical and Materials Engineering**

Prof. Dr. M. Kadri Aydınol _____
Supervisor, **Metallurgical and Materials Engineering, METU**

Examining Committee Members:

Prof. Dr. İshak Karakaya
Metallurgical and Materials Engineering, METU _____

Prof. Dr. M. Kadri Aydınol
Metallurgical and Materials Engineering, METU _____

Prof. Dr. Arcan Dericioğlu
Metallurgical and Materials Engineering, METU _____

Assist. Prof. Dr. İlkay Kalay
Materials Science and Engineering, Cankaya University _____

Assist. Prof. Dr. Simge Çınar
Metallurgical and Materials Engineering, METU _____

Date: _____

I hereby declare that all information in this document has been obtained and presented in accordance with academic rules and ethical conduct. I also declare that, as required by these rules and conduct, I have fully cited and referenced all material and results that are not original to this work.

Name, Last Name: EMRE YILMAZ

Signature :

ABSTRACT

DEVELOPMENT AND CHARACTERIZATION OF TIN BASED ANODE MATERIALS FOR LI-ION BATTERIES

Yılmaz, Emre
M.S., Department of Metallurgical and Materials Engineering
Supervisor : Prof. Dr. M. Kadri Aydınol

February 2018, 67 pages

Li-ion batteries are the most popular type of portable secondary batteries. They generate electrons at anode electrode during discharging process by releasing Li^+ ions from anode, in which graphite is used as Li reservoir. Recently, SiO_2 and Tin (IV) Oxide materials are investigated as anode materials by researchers, due to their very high theoretical capacity. There are two problems, however, limiting their use which are pulverization and irreversible reaction problems. These problems are, also, the causes of the capacity loss during charge-discharge cycles. To solve these problems, tools of nanotechnology are used to obtain different nanostructures. Doping with elements is another way to improve properties. In this study, tin based anode materials was developed for lithium ion batteries. For the production of materials, hydrothermal method was used. The effect of hydrothermal processing parameters and alloying elements such as La, W, Y and Zr were investigated. Produced materials were characterized by SEM, TEM also XRD for structural analysis and EDS were used for chemical analysis. Samples will be assembled in coin cells and galvanostatic charge-discharge, cyclic voltammetry and electrochemical impedance spectoscopy techniques were applied for their electrochemical characterization.

Keywords: Li-ion batteries, Anode materials, Tin oxide

ÖZ

LİTYUM İYON PİLLERİ İÇİN KALAY BAZLI ANOT MALZEMELERİNİN ÜRETİMİ VE KARAKTERİZASYONU

Yılmaz, Emre
Yüksek Lisans, Metalurji ve Malzeme Mühendisliği Bölümü
Tez Yöneticisi : Prof. Dr. M. Kadri Aydınol

Şubat 2018 , 67 sayfa

Lityum iyon pilleri taşınabilir şarjedilebilir piller arasında en popüler olanıdır. Anot malzemesi olarak grafit kullanılan bu tip pillerde, enerji tüketimi sırasında lityumun depolandığı anottan lityum iyonu salınımı gerçekleştirilerek elektron üretimi sağlanır. Son zamanlarda, yüksek teorik kapasitelerinden dolayı, SiO_2 ve Tin (IV) Oxide de anot malzemesi olarak araştırılmaya başlanmıştır. Geri dönüşümsüz tepkimeler ve malzemenin tozlaşması bu pillerin kapasitelerini kısaltmaktadır. Ayrıca bu problemler pillerin, her bir şarj etme – kullanım döngüsünden sonra performansının düşmesine de sebep olmaktadır. Bu problemleri çözmek için, nanoteknoloji kullanılarak farklı yapılar üretilmekte ve farklı elementlerle alaşımlamak da önerilmekte. Bu çalışmada, lityum iyon pilleri için kalay bazlı yeni anot malzemesi üretilmiştir. Malzeme üretimi için hidrotermal yöntem kullanılmıştır. Hidrotermal işleminin parametrelerinin ve La, W, Y ve Zr gibi alaşım elementlerinin etkisi araştırılmıştır. Üretilen malzemelerin SEM, TEM ve XRD ile yapısal analizi, EDS ile kimyasal analizi yapılmıştır. Düğme pil olarak üretilen bu pillerin galvonastatik şarj-deşarj, döngüsel volt ölçümü ve elektrokimyasal iç direnç spektropisi teknikleri uygulanarak elektrokimyasal karakterizasyonu da sağlanmıştır.

Anahtar Kelimeler: Lityum iyon pilleri, Anot malzemeler, Kalay oksit

TABLE OF CONTENTS

ABSTRACT v

ÖZ vi

TABLE OF CONTENTS vii

LIST OF TABLES x

LIST OF FIGURES xii

CHAPTERS

1 INTRODUCTION AND THEORETICAL BACKGROUND 1

1.1 Lithium-ion Batteries 1

1.1.1 Introduction and the History 2

1.1.2 Basic Principles 4

1.2 Materials 6

1.2.1 Cathode Materials 6

1.2.2 Anode Materials 10

1.2.3 Electrolyte Materials 20

1.3 Problems of Anode Materials in Li-ion Batteries 22

1.3.1 Solutions 23

1.3.1.1 Nanostructured Materials 23
1.3.1.2 Alloying with Active Materials 26
1.4 Hydrothermal Treatment and Formation of Tin Oxides 28
2 EXPERIMENTAL PROCEDURE 33
2.1 Hydrothermal Processing of Materials 33
2.2 Crystallographic and Morphological Characterization 36
2.3 Electrode Fabrication and Measurements 37
3 RESULTS AND DISCUSSION 39
3.1 Qualitative Analysis of the Products 39
3.2 Quantative Phase and Yield Analysis of the Products 39
3.3 Crystallographic and Morphological Characterization 41
3.3.1 Effects of Processing Time and Concentration . . . 41
3.3.1.1 Morphology 41
3.3.1.2 Dominant Phase 43
3.3.2 Effects of pH Value 43
3.3.3 Effects of Water:Ethanol proportion 46
3.3.4 Effects of Heat Treatment 49
3.3.5 Effects of $K_2S_2O_8$ 50
3.3.6 Effects of Alloying 51
3.4 Electrochemical Characterization 52
3.4.1 Cyclic Voltammetry 52

3.4.2 Charge Capacity and Voltage Profile 53

4 CONCLUSION 57

REFERENCES 59

LIST OF TABLES

TABLES

Table 1.1 Various rechargeable batteries and their average cell potentials [1]. . 2

Table 1.2 Influence to the particle size of the temperature in the aqueous solution treated for 24 hours. 25

Table 1.3 Shape and dimensions of tin oxide structures prepared with different surfactants. 26

Table 2.1 Experiments: Concentration is less than 0.1 moles. 34

Table 2.2 Experiments: Concentration is 0.1 moles, water-ethanol proportion higher than or equal to three to one. 35

Table 2.3 Experiments: Concentration is 0.1 moles, water-ethanol proportion lower than three to one. 35

Table 2.4 Experiments: Chosen experimental procedure for Tin (IV) Oxide and Tin (II) Oxide. 35

Table 2.5 Experiments of alloying tin oxide with La, Y, W and Zr. 36

Table 2.6 Parameters of experiments on tin oxide production using $K_2S_2O_8$ as oxidation agent. 36

Table 3.1 Results: Concentration is less than 0.1 moles. 39

Table 3.2 Results: Concentration is 0.1 moles, water-ethanol proportion lower than three to one. 40

Table 3.3 Results: Chosen experimental procedure for Tin (IV) Oxide and Tin (II) Oxide. 40

Table 3.4 Results: Concentration is 0.1 moles, water-ethanol proportion higher than or equal to three to one. 40

Table 3.5 Results of alloying tin oxide with La, Y, W and Zr. 41

Table 3.6 XRD test results of experiments on tin oxide production using $K_2S_2O_8$ as oxidation agent. 41

LIST OF FIGURES

FIGURES

Figure 1.1 Schematic representation of a typical lithium-ion battery cell [2]. . 5

Figure 1.2 Effect of the morphology [3]. Bulk tin is presented with hollow points and mesoporous tin material is presented with solid points. 24

Figure 1.3 Effect of particle size [3]. 24

Figure 1.4 SEM images of the products treated for 6(a), 12(b), 18(c) and 24(d) hours at 180 ^{o}C. 25

Figure 1.5 Effect of alloying with cobalt [3], 18650 Nexelion Sony battery. Sputtered powder and sputtered film curves are irrelevant. Alloyed tin curves show stability and cyclability unlike pure tin and tin oxides. 28

Figure 3.1 XRD diagrams of Sn01pH24(A) and Sn01pH24t12(B). Same solution is prepared for A(Sn01pH24) and B(Sn01pH24t12), concentration of tin ions in the solution of C(SnWaterpH21) is ten times higher concentrated. Hydrothermal treatments are prolonged 3 hours for Sn01pH24 and SnWaterpH21, 12 hours for Sn01pH24t12. 42

Figure 3.2 Dependence of the composition of the phases on concentration of $SnCl_2.2H_2O$ in the solution. When concentration decreases, formation of Tin (IV) Oxide is favored. Circles refer to 0.01 moles while squares refer to 0.1 moles of tin precursor is used. 43

Figure 3.3 Changing thickness of Tin (II) Oxide microsheets with changing pH value. From left to right, specimens are SnWaterpH86, SnWaterpH95 and SnWaterpH101. 44

Figure 3.4 Comparison between those three specimens, SnWaterpH86(A), SnWaterpH95(B) and SnWaterpH101(C). Shifting peaks is caused by morphology and texture. 45

Figure 3.5 Comparison of SEM images between two specimens which they are produced with different pH values. Left: SEM image of SnWaterpH30(pH=3.0), wtr:EtOH=1:0, magnification 5000x. Right: SEM image of SnWaterpH86(pH=8.6), wtr:EtOH=1:0, magnification 5000x. 45

Figure 3.7 Comparison between those three specimens, SnWaterpH30(A) and SnWaterpH101(B). Shifting peaks is caused by morphology and texture. . 46

Figure 3.8 Dependence of composition of the phases on water-ethanol proportion of the solution. For all solutions, 0.1 moles $SnCl_2.2H_2O$(the molarity is 71.4mM) is used. Circles for Water:EtOH=1:0, squares for Water:EtOH=3:1 and diamonds for Water:EtOH=1:3. 47

Figure 3.9 In same concentration and pH values are chosen, pure ethanol in SnEtOHph17(A) and pure water SnWaterpH21(B) are used as solvents. As we can see crystallization is at higher degree at SnWaterpH21. 48

Figure 3.10 Comparison between two specimens which they are produced with different solutions according to their water-ethanol proportion in acidic environment. Left: SEM image of Sn19ph19, wtr:EtOH=3:1, magnification 5000x. Right: SEM image of SnEtOHph17, wtr:EtOH=0:1, magnification 5000x. 48

Figure 3.11 Comparison between two specimens which they are produced with different solutions according to their water-ethanol proportion in basic environment. Left: SEM image of Sn21ph80, wtr:EtOH=3:1, magnification 5000x. Right: SEM image of SnWaterpH86, wtr:EtOH=1:0, magnification 5000x. 49

Figure 3.12 XRD diagrams of the specimens Sn19ph19 and heat treated Sn19ph19. 49

Figure 3.13 HRTEM images of SnEtOHph17(left) and SnK2S2O8EpH09(right). Crystalline sizes are 5nm in diameter. 51

Figure 3.14 XRD diagrams of SnEtOHph17(A) and SnO2K2S2O8E(B). 51

Figure 3.15 CV measurement 52

Figure 3.16 Charge densities versus charge-recharge cycles for tin monoxide group. 53

Figure 3.17 Charge densities versus charge-recharge cycles for tin dioxide group. 54

Figure 3.18 Discharge-time profile for alloyed and pure SnO 54

Figure 3.19 Discharge-time profile for alloyed and pure SnO_2 55

CHAPTER 1

INTRODUCTION AND THEORETICAL BACKGROUND

1.1 Lithium-ion Batteries

Batteries are cells that can store the energy in electrochemical form, and they are used in devices that require energy in various applications. The batteries can be basically classified into two categories:

1. Primary Batteries: This type of battery converts the chemical energy into electrical energy. The electrochemical reaction is not reversible and the battery cannot be used after it is fully discharged. Thus, this type of battery is preferred for devices that require high energy density for a single use.

2. Secondary Batteries: This type of battery is also known as Rechargeable Battery. The electrochemical reactions in this type of battery is reversible. After being discharged, the battery can be recharged with external power. This type of battery converts the chemical energy into electrical energy during discharge, also convert the electrical energy into chemical energy during charge. In both cases, some of the energy is converted into heat energy inside the battery. In a full cycle, the efficiency of the battery varies approximately between 80-90%.

The cell is made up of positive and negative electrode plates which are insulated from each other, and an electrolyte that provides conductivity between the plates. Both groups of electrodes are connected to two terminals. These cells can store energy at very low electrical potentials. The capacity of a typical cell is defined by Ampere-hour (Ah). An ampere-hour denotes the amperage that a cell can give. The battery

is made up of several cells which are connected in parallel or series to each other for the desired current or voltage values. For example, the device using the battery has to contain a large number of batteries connected in series to each other for both high voltage values and high amperage values. Rate of the battery charge during use is calculated by average voltage values. Charge and discharge rates of the battery are determined by considering its Ampere-hour capacity value.

Today, the six major types of rechargeable batteries which have been commercialized can be listed as follows:

1. Lead-Acid (Pb-Acid),
2. Nickel-Cadmium (NiCd),
3. Nickel-Metal Hydride (NiMH),
4. Zinc-Air,
5. Lithium Ion (Li-Ion),
6. Lithium Ion Polymer.

The average voltage rates of the batteries during discharge based on their electrochemistry are shown in Table 1.1.

Table 1.1: Various rechargeable batteries and their average cell potentials [1].

Electrochemistry	**Voltage (V)**	**Description**
Lead Acid	2.0	The cheapest technology
Nickel Cadmium	1.2	Shows memory effect
Nickel Metal Hydride (NiMH)	1.2	Sensitive to temperature
Lithium Ion	3.4	Safe, does not contain metallic Lithium
Lithium Polymer	3.0	Contains Metallic Lithium
Zinc Air	1.2	Requires proper air management system.

1.1.1 Introduction and the History

Compared to all rechargeable battery systems, lithium-ion batteries are the systems that have the highest power. They are used as power supplies for the most popular electronics such as cameras, laptops and mobile phones. The fundamental reasons

why they are preferred are that they are lightweight, have flexible usage and longer service lives.

Nowadays, the studies on increasing the energy density, cycle life and safety of batteries continue to be conducted. When we look at the commercial sector, lithium-ion batteries are preferred in almost all electronic devices that require batteries due to their superior performance.

In the past, the studies were carried out on the use of lithium metal, which has the highest electronegativity as the anode material in rechargeable batteries and is one of the lightest elements (6.94 g/mol). The first battery with lithium anode electrode was produced in 1970. Indeed, these batteries had a very high capacity, and in a short time, they were presented for use with clocks, calculators and portable medical devices. The first studies on lithium-ion batteries were conducted by Exxon group. In the battery they developed, TiS_2 was used as positive electrode, lithium metal as negative electrode, and perchlorate in dioxolane as the conductive electrolyte [1]. TiS_2 compound had a very stable structure and was susceptible to reversible reaction with lithium. However, many problems have arisen after its use. The main reason was the growing dendritic structures on the surface of the lithium metal electrode. The reason for their formation was the interaction between electrolyte and lithium metal. It was observed that the growing dendrites penetrate the separator and caused short circuits in time, and these short circuits caused combustions and burstings. After these kinds of problems, instead of lithium metal, the studies have focused on different type of materials and lithium-aluminum alloy [4]. With the study they carried out in 1971, Dey et al. have proven that lithium alloys carried out electrochemical reactions inside the organic electrolytes [5]. From that day on, alternatively, many anode materials have been produced. When compared to that of pure lithium metal, the energy densities of lithium alloys have become two or three times lower [6]. Besides this, the electrochemical energy occurred at the entry or exit of the lithium metal into/from the alloy matrix has been insufficient. This has caused a faster deterioration in the integrity of the alloy anodes, also in time, cracks and fragmentation in the anodes. The service life of the rechargeable lithium-ion batteries using lithium alloys as the anode material was, owing to this, very low. In the later studies, it has been observed that the graphite was dimensionally quite stable. With the formation of LiC_6 compound

formed by the entry of lithium into the carbon structure, it has been observed that the distance between the layers was, at most, 10%. For this reason, the graphite is used in lithium-ion batteries as the only substitute of lithium metal and its alloys today. In addition to this, the studies on the substitute materials of heavier halides - such as oxides - have also been successful [7].

Goodenough et al. have produced a number of cathode materials belonging to Li_xMO_2 family (M = Co, Ni or Mn) [8]. By the end of 1980s, the production of lithium-ion batteries with proper anode, cathode and electrolyte compatibility had been fully realized. The components of lithium-ion batteries were first fully explained by Murphy [9] and then by Scrosati et al [10].

Ultimately, lithium-ion battery was first introduced to the market by Sony [11]. Nowadays lithium-ion batteries are frequently used in consumer electronics, military applications, space and especially wireless communication technology.

1.1.2 Basic Principles

The process concept of a basic lithium-ion battery system was described as partially concentrated cells containing relatively similar electrodes with different reactors [12]. Later on, this concept was changed to anodes and cathodes containing metal compounds [13].

A basic lithium-ion battery is made up of a positive electrode (cathode), a negative electrode (anode), an electrolyte (liquid or solid) containing dissolved salts, and a separator that separates two electrons. Lithium-ions provide a constant flow between the electrodes. The basic working principle of lithium-ion batteries is shown in figure 1.1. During the discharge process, lithium-ions separate from cathode, pass through the separator via electrolyte, and form a compound with the anode material. Similarly, the electrons released from cathode are held by the anode material via an external circuit. The charging process takes place in the opposite state. In order to achieve high efficiency and long cycle life during cycles, it is extremely important that the lithium-ions in the anode pass to the cathode material without causing any damage or making any changes in the crystal structure. In order to obtain a very high operating

voltage in the design of a lithium-ion battery system, it is extremely important to choose the right electrode pairs and electrolytes. A high operating voltage is obtained by very small high-efficiency anode and cathode electrodes.

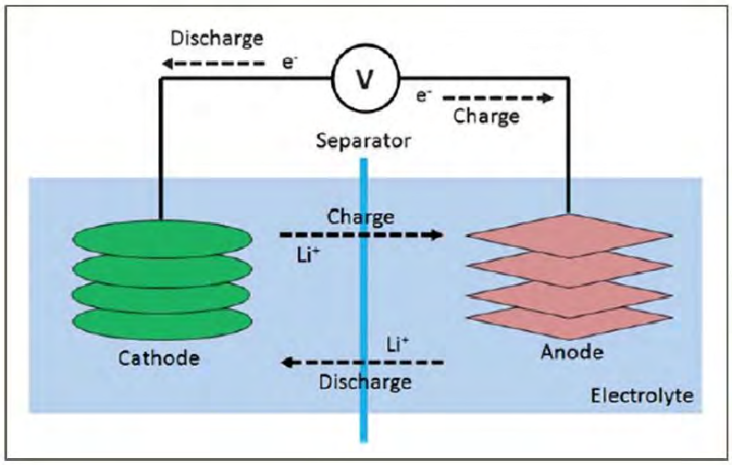


Figure 1.1: Schematic representation of a typical lithium-ion battery cell [2].

The carbon (hard carbon or graphite) used as the anode material in lithium-ion batteries has a potential ranging from 0 to 0.8 V. As cathode materials, $LiMn_2O_4$, layered $LiCoO_2$ and $LiNiO_2$ materials with 4 V potential are generally preferred. A lithium-ion battery with high cathode potential and low anode potential approximately has a potential ranging from 3.6 to 3.8 V. This potential value is exactly three times higher than that of Ni-Cd and Ni-MH batteries.

When we look at the literature, we can see that significant studies have been conducted on the anode and cathode materials used in lithium-ion batteries for the last 25 years. The studies have especially concentrated on lithium metal, lithium binary alloys, carbon and metal oxide composites. In the studies carried out until today, graphite is found to be the best choice out of all anode materials in terms of performance and service life.

1.2 Materials

1.2.1 Cathode Materials

In rechargeable lithium-ion batteries, cathode electrodes serve as a source for lithium-ions that will go to the anode. Accordingly, the physical, structural and electrochemical properties of cathode materials have a great impact on the overall performance of the battery. The basic properties of cathode materials can be listed as follows:

1. The discharge reaction needs to have the highest negative Gibbs free energy possible (high discharge voltage).
2. The structure of the cathode material should have a low molecular weight and be able to release the lithium-ion at high rates during discharge (high energy capacity).
3. The cathode material should have a high lithium chemical diffusion coefficient (high power density).
4. Structural changes during charge and discharge should be as low as possible (long cycle life).
5. The materials should be chemically stable, cheap and have no toxic effects.
6. Moving or handling the materials should be as easy as possible.

The first material to be proposed as a cathode material was TiS_2. Later on, chromium and vanadium oxides have also begun to be used [14]. In addition to this, many of the compounds proposed for the cathode material in the literature are quite limited due to critical requirements such as high energy density, good cycle life and safety. Generally, layered $LiMO_2$ (i.e. $LiCoO_2$, $LiNiO_2$, $LiMnO_2$) compounds, manganese oxides (i.e. $LiMn_2O_4$ spinel) can be given as examples for the cathode materials with higher energies than 3 V [14].

Today $LiCoO_2$ is the most frequently used cathode material. T. Ohzuku [15] examined the reaction mechanisms of $LiCoO_2$ cathode material by using the XRD techniques and stated that $LiCoO_2$ electrode material could be separated into three dif-

ferent areas. It was discovered that $Li_{1-x}CoO_2$ cathode material had two hexagonal structures in the $0 < x < 1/4$ area. It was observed that a two-phase structure occurred in the area as a result of the addition or subtraction of lithium and the resulting structure in the $1/4 < x < 3/4$ area had single-phase [16]. Theoretically, the separation of lithium from 1 mol $LiCoO_2$ yields an energy of 274 mAh/g. However, when only a portion of lithium is taken into account in terms of structural integrity, only limited part of the lithium can reversibly separate from the cathode and returns. Approximately 1000 charging/discharging cycles can be successfully achieved with the capacity of $LiCoO_2$cathode material [16].

Another cathode material on which the studies concentrated is $LiNiO_2$, and its thermal stability is especially low in highly oxidized form. With the separation of one half mole of lithium from $LiNiO_2$, two cubic spinels of $LiNi_2O_4$ are formed and this structure has a very high stability. Therefore, the amount of Li^+ that should be separated from cathode and its mobility are reduced. Owing to these limitations, the use of $LiNiO_2$ compound as a cathode material is practically impossible [16].

The theoretical capacity of $LiNiO_2$ compound is close to 275 $mAhg^{-1}$, when compared with $LiCoO_2$. In practice, when charged with a value between 4.1 and 4.2 V, it reaches a value between 185 and 270 $mAhg^{-1}$. This value is even higher than that of $LiCoO_2$ cathode. However, the cycle lives of $LiNiO_2$ electrodes are shorter. These studies have shown that the electrochemical power, structural stability, specific power and average charge/discharge of the $LiNiO_2$ compound have changed over time. The reason for this was that the lithium-ions in spinel structure were settling into octahedral spaces [17].

There are many publications and patents on various applications of doping on the $LiNiO_2$ compound today. Ti, V, Cr, Fe, Co, Mn, Cu, Zn, Cd, Sn, Al, B, Mg, Ga, Ca and Na can be given as examples. Nowadays, the cathode production has been focusing on adding new ones to the multiple systems mentioned above and the advantages that each compound will bring to reversible reactions.

The spinel $LiMnO_4$ belonging to the cubic system is in a crystal structure in which Li^+ ions are in tetragonal, $Mn^{+3/+4}$ ions are in octahedral, and O^{-2} ions are in octahedral spaces. Electrodes with similar crystal structures have very high electro-

chemical cycles. For example, spinels can be highly tolerable towards the cycles in unit cells. Electrode of the Li-Mn-O spinel has a capacity of 4 V. $Li_{1+x}Mn_2O_4$ electrode has two crystal structure. These are $LiMn_2O_4$ and $Li_2Mn_2O_4$ with cubic and tetragonal structure. In $LiMn_2O_4$ spinel, the structural integrity of the electrode is maintained thanks to strong Mn-O bonds at the exit and return of the lithium-ions. In time, however, a cubic structure gradually replaces the tetragonal structure. This phase change causes changes in the crystal structure of the electrode and deteriorations in its electrochemical properties by causing volumetric changes in each unit cell of the electrode. In important aspects such as capacity and rechargeability, $LiMn_2O_4$ electrochemical properties of spinel vary depending on the production methods. $LiMn_2O_4$ spinels synthesized at low temperatures have high capacities and low cycle lives. $LiMn_2O_4$ spinel - generally obtained by solid-solid reactions - has a discharge capacity of 120-140 $mAhg^{-1}$, which is a very good loop cycle. In the tin-rich $Li_{1+x}Mn_{2-x}O_4$ spinels, the capacity decreases are reduced at a high rate. In addition to this, at higher temperatures, the degradation is still much worse than that in nickel or cobalt-rich materials. The life cycle of $LiMn_2O_4$ spinel can be increased with the addition of elements such as Li, Mg, Zn, Co, Cr, Al and Ti.

Besides this, with the increase of the metal concentration, various decreases have been observed in the capacity. Robertson and his study group [18] have examined the effect of metals - such as B, Cr, Fe, Ti, Al and Ga - on the single-phase $Li_{1+x}Mn_{2-x}O_4$ spinel. Their studies have shown that the best doping effect has been achieved by the addition of Cr. In addition to obtaining a reversible capacity of 110 $mAhg^{-1}$, no capacity change was observed during the first hundred cycles. The reasons for this can be the ionic structure, the orientation of crystal structure and the stability of oxidation.

Successful results have been achieved by the addition of cobalt into $LiMn_2O_4$ spinel. $LiCo_{1/6}Mn_{11/6}O_4$ spinel has shown the best performance in terms of capacity and cycle life. In the three hundredth cycle, the energy density of the cathode for the Li/$LiCo_{1/6}Mn_{11/6}O_4$ cell has been calculated as approximately 370 Wh/kg [18]. With the addition of Co into $Li_xMn_2O_4$ spinel, there has been an increase in its grain size, and its overall surface area has been reduced by half. When the Co content was changed between y=0 and y=0.06, there have been very high increases in the first

capacity of $LiCo_yMn_{2-y}O_4$ spinel. The lithium-ion diffusion coefficient in the Co doped spinel has changed between 2.4×10^{-12} and $1.4 \times 10^{-11} m^2/sec$. These values are much higher than that of a pure spinel by (9.2×10^{-14} and $2.6 \times 10^{-12} m^2/sec$). Moreover, the increase in the grain size of Co doped into the spinel also causes a decrease in the contact between the active materials and the electrolyte, resulting in the discharge phenomenon at a lower rate [18].

One of the most important reasons for the increases in the cycle performance is the enhanced stability of the octahedral spaces in the spinel. The bond energies of MnO_2, CrO_2 and CoO_2 are respectively 946, 1142 and 1067 kJ/mol. Depending on these values, it can be said that M-Cr and M-Co bonds are much stronger than M-O bonds [18].

Other developed cathode materials are lithium vanadium oxide and vanadium oxides in lithium-ion batteries. Lithium metal is used as an anode in lithium-ion polymer batteries. Because of the direct use of lithium in anode, it is necessary to use a lithium-containing metal in the cathode. For this reason, vanadium oxides are cathode materials which are in demand for lithium-ion polymer batteries since they have high specific energy and voltage values ranging between 2 and 3 V. Crystalline V_2O_5 [19], amorphous V_2O_5 [20] and $V_2O_5 - B_2O_3$ with V_2MoO_8 [21] compounds have also been studied intensively. It has been found that the discharge voltages of the cathodes were approximately 2.5 V. Since the capacity decreased during the cycles, mass production of these cathode materials has not been introduced. In the last studies, $Li_xFe_yO_z$ (Li^+/Fe^{+3}=0.69) compound was synthesized and, after electrochemical measurements, it has been found that the specific capacity of the electrode material was 140 mAh/g and its discharge voltage was 2 V [22]. When the low cost of Fe is taken into account, it is certain that this electrode will be among the popular cathode materials. Padhi and his study group have developed an olivine-based ($M - SiO_4$) cathode material [23]. In another study, Li_3FePO_4, $LiFeP_2O_7$, $Fe_4(P_2O_7)_3$ and $LiFePO_4$ compounds were examined and it was observed that the specific capacity of the $LiFePO_4$ compound was 130 mAh/g and the average cell voltage was over 3.3 V. In order to increase the discharge voltage, $LiCoPO_4$ compound was prepared and its cyclic behavior was examined [24]. Even though the average voltage was increased to 4.5 V, it wasn't a great success because of the elec-

trode deteriorations.

1.2.2 Anode Materials

Prior to rechargeable lithium-ion batteries, lithium was used as the anode material for primary batteries. With the introduction of lithium-ion secondary batteries, a high energy density has been obtained due to lithium having the highest capacity among the available preferences. However, the rechargeable lithium batteries caused great failures in the first attempts. The most important reason for this was the safety problems caused by the anodes produced with pure lithium metal. After charge and discharge, the formation of dendritic growths was observed in the lithium anode. These dendritic structures were highly porous, had a large surface area and were able to interact with organic electrolytes. In addition to that, it had been observed that dendritic structures, which were gradually forming in the lithium metal, continued to grow throughout the cycles, and reached the separator that separates the anode and cathode. As a result, the short circuits occurred in the batteries, and these short circuits could even cause the batteries to burst or combust. These problems were overcome in a very short time by the discovery of various alloying elements such as graphite, Sn, Al, Pb, Bi, Sb, and As. Also, some oxides such as $Li_4Ti_5O_{12}$ and perovskites can form compounds, which have relatively low potentials, with lithium. There are three basic requirements for an anode material;

1. The anode electrode should have the capacity to form reversible compounds with lithium,
2. For a high specific capacity, the anode material should form a compound with the maximum amount of lithium,
3. For a high cycle life, anode electrodes should form convertible compounds with lithium metal.

Today, carbon is used as an anode material in the rechargeable battery industry. As an anode material for lithium-ion cells, carbon has very important properties. In the history of the development of lithium-ion batteries, the successful use of carbon anodes and their commercialization are highly striking. The first use of graphite as an

anode material was a major failure due to its fragmentation. However, it has been determined that carbon anodes produced in low crystallinity state showed less reactivity towards the electrolyte solution. The first production of lithium-ion battery by using non-crystalline carbon anodes was carried out by Sony in 1990 [25].

Today, many carbon types containing natural and synthetic graphites, carbon black, active carbon, and carbon fibers can be commercially produced in an inert gas atmosphere by using various organic precursors. For this reason, carbon materials used as anode materials have many structures, textures and morphological properties [26].

Dahn and his group have conducted studies on a variety of carbon materials that could be used in lithium-ion batteries [27]. The first of these was the graphitic carbons obtained by processing carbon compounds at about 2400 ^{o}C. The second was hydrogen-containing carbons prepared from organic compounds pyrolyzed at 700 ^{o}C. The third was the anode materials obtained by the synthesis of hard carbons. The structure and chemistry of the resulting carbons highly depend on the operation conditions of the organic compounds. By fragmenting organic components in the inert gas atmosphere and below 600 ^{o}C, CO and CH_4 gases are brought out. The remaining carbon atoms precipitate in the form of planar aromatic structures (graphene structure). In the event of fragmentation of gas into a semi-liquid state, these planar plates are arranged in a more parallel structure. This makes graphitization easier as the temperature increases. Similar compounds enable the formation of graphite carbons. However, if the organic components have sufficient cross-links, the flow state cannot be achieved and no planar aromatic structures are formed. The graphitization of these kinds of carbon materials is impossible at high temperatures, and hard carbon is obtained as a result. All carbon materials processed between 1300 and 1500 ^{o}C have graphite-like hexagonal structures [28].

The theoretical capacity of Graphite LiC_6 formation is 372 mAh/g [29].

$$6C + Li^{+}e^{-} \rightarrow LiC_6 \tag{1.1}$$

The charge during the first reaction is usually above the theoretical capacity. At the same time, it can be said that the reason for this is a secondary reaction in the electrolyte. Electrolyte separation is caused by the exfoliation of graphite, and this leads to a decrease in the reversible reactions in the anode. According to this, if the elec-

trolyte that is going to be chosen is suitable for the anode materials, the damage to a similar battery will be decreased.

Also, throughout the first cycle, a passivation film called solid-electrolyte interface (SEI) will be formed on surface of the anode. The formed interface is not electrically conductive but ionically conductive. This interface prevents any damage to the electrolyte as well as the deterioration of the electrolyte. Even under the voltage levels which cause many electrolytes to lose their stability, the formation of the passivation layer preserves the stability and cycle life of the carbon electrodes [65].

The reaction behaviors of lithium with hard carbon electrodes such as coke, show a number of differences compared to that of the graphite electrodes. Unlike that of graphite, the cyclic profiles of hard carbon electrodes occur on a straight line ranging from 1.2 V to 0.2 V, rather than in the curves traveling on top of each other. It is believed that by the addition of lithium to hard carbon, the spaces in the hard carbon are filled by lithium. As a consequence of this, weak lithium-carbon bonds appear, and consequently, experimental results yield low capacities. The carbon layers have monolayer structure in hard carbon materials, partly like houses made of cards. In this single layer, lithium-ions enter from every side so that they can react with the carbon atoms (LiC_6) more. This causes the theoretical capacity to reach a value of approximately 327 mA/h. In irregular coke electrodes, the reaction process does not allow the stacked phases to form. Due to lack of crystalline structure, these electrodes cannot exactly match the electrolytes just as they cannot match the graphite electrodes. Carbon anode materials obtained from coke are commercially used in the Sony video cameras today [30].

When the hydrogen-containing carbon electrodes are considered, their capacity increases about 800 - 900 mA/h. Hydrogen plays an important role in the reaction with lithium. With the increasing atomic H/C ratio in these materials, reversible capacity has also increased. When they encounter a hydrogen atom, the lithium ions entering the structure cause changes in the C-H bond by sharing electrons with the hydrogen. However, when their long-term use is considered, the cycle lives of carbon-hydrogen electrodes do not seem very long [31].

Works on the development of the specific energies and cycle lives of carbon anode

materials still continue. In the studies that have been carried out, it has been discovered that the capacity of some part of the carbon-based materials - obtained by the pyrolysis of specific compounds - is 1000 mAh/g. The nanocrystalline carbons obtained by using high energy ball mills was observed to have a capacity of 2500 mAh/g in the first charge. However, half of the reversible capacity was lost only in the first charge. In practical applications, when the existing devices are considered, obtaining such a high energy in the first charge is not favorable. However, the target is carbon electrodes to have a value between 600 - 700 mAh/g and long cycle life [32].

Although a development in both electrode systems is necessary, the main limitation of lithium-ion batteries that are commercialized today is caused by the anode, which is a negative electrode. In lithium-ion batteries, lithium metal was first used as a negative electrode and this resulted in very high voltages and specific energy values. However, due to the dendritic growth of lithium over time and the high temperatures during the reactions, first batteries had a high combustion risk [33].

The graphite - which is micron-sized and has powder form - is the most popular negative electrode material used in rechargeable lithium-ion batteries. After lithium-ion compounds with carbon and LiC_6, theoretically a specific energy of 372 $mAhg^{-1}$ is obtained. However, a maximum specific energy of 170 $mAhg^{-1}$ was obtained in the commercial applications of the negative electrodes made out of graphite, which was micron-sized and in powder form [34]. However, the studies that have been conducted in recent years have shown that especially with the use of nano-sized graphite, the number of lithium-ions in the anode electrode has increased, and as a result, the battery capacity has also highly increased [35]. With the high increases in the battery capacity, however, the service life of the battery decreased. Especially the passivation layer (SEI) which is formed on the surface of the electrolyte, causes cracks and spillage on the electrolyte in time, thus making the battery unusable [36]. Therefore, electrode materials with much higher energy densities, longer cycle lives and higher safety must still be developed for the rechargeable lithium-ion batteries.

Metal oxides and halogenoids such as MoO_2 [37], WO_2 [38] and TiS_2 [39] were used as negative electrodes in the first developed lithium-ion cells. Also, when they were used with positive electrodes in a battery cell, a relatively low cell voltage had

occurred. Nowadays negative electrode studies have been focusing on lithium alloys and compounds, TiO_2, Si and SnO_2 - especially because of their high theoretical capacity values.

It has been observed that the particularly prominent material types in the studies conducted on lithium-based negative electrode materials, are LixMVO4 (M = Co, Cd, Ni, Zn; 1 < x < 8) [40], MnV_2O_6 [41] and the lithium nitrate [42] compounds. However, since their production is highly complex and expensive, these types of electrodes do not have any commercial value yet.

The use of lithium alloys as a negative electrode in lithium-ion battery cells, instead of lithium, first started with the study of Dey [43]. Based on Dey's study, the charging and discharging operations of lithium alloys can be explained with this equation;

$$Li_xM \rightarrow xLi^+ + xe^- + M \tag{1.2}$$

Except for a few exceptional cases (i.e. M = Ti, Ni, Mo and Nb), alloys of lithium and other metals are obtained at relatively low temperatures. When electrode reactions are taken into consideration, however, it has been observed that Li_xM compound has a very wide compound range [44].

The most important metals capable of electrochemically alloying with lithium can be listed as aluminum, silicon, tin, lead, indium, bismuth, antimony and silver [45]. As a result of the alloy of these metals with lithium, however, significant changes occur in the matrix metal. Especially in the electrochemical studies of lithium, it has been observed that many phases occurred. In the studies that have been carried out, α-phased ($LiAl$ compound containing lithium approximately at the rate of %7) and β-phased (non-stoichiometric $LiAl$ compound containing lithium between 47-56%) and various lithium-rich $LiAl$ phases were obtained as a result of the electrochemical interaction between aluminum and lithium [4]. During the discharge process, while the $LiAl$ alloy in the α-phase did not show any reversible reaction, the $LiAl$ alloy in the β-phase showed a complete reversible reaction [46].

Generally, the charge densities of lithium alloys are considerably high. In the lithium-rich phases at room temperature, however, Li^+ ion diffusion is relatively high, and can produce high current values during charge/discharge [46]. Nevertheless, the prob-

lems caused by the high volumetric expansion after making a compound with lithium cannot be solved. For this reason, the current studies have particularly focused on the metallurgical properties and morphological structures (grain size, grain shape and preferential orientation) of lithium-alloy electrode materials [47]. The electrodes produced from alloys with micron grain structures cannot tolerate the volumetric expansion that occurs throughout the charge and discharge cycles. However, it has been observed that the cycle capacities are further enhanced in the electrodes produced in thin film form [6]. Besides, when compared with the gravimetric capacity achieved with the total electrode mass, it has been observed that the total capacity is rather low [48].

It is known that there are intensive studies going on particularly on the production of oxide-based nanotubes and nanowires [49]. Particularly in photovoltaic, photocatalytic, semiconductor, catalytic and gas sensor applications, it is known that great efforts have been made for the production of TiO_2-based nanotubes [50]. It is also known that TiO_2-based materials are used as negative electrode materials in lithium-ion batteries [51]. Regarding the electrode materials of the lithium-ion batteries, it is a well-known fact that especially nanotube morphology has great advantages [52]. The synthesis of TiO_2 in the form of nanotube, has proven that the nanotubes obtained from the first studies are actually $Na_yH_2 - yTi_nO_{2n+1}.xH_2O$. Later on, based on the TiO_2-B polymorph, obtained nanotubes have much lower density than that of the other polymorphs of TiO_2, which are rutile, anatase and brookite. Thanks to this, lithium-ions and electrons can pass through the nanotube in a controlled manner, especially in lithium-ion battery applications. As a result of the reaction of the TiO_2 (B) produced in the form of nanotube with the lithium, $Li_{0.91}TiO_2$ (B) compound has been produced and a specific energy of 305 mAh/g has been obtained. Another advantage of the $Li_{0.91}TiO_2$ (B) compound is that there is no deformation in nanotubes. In the electrode applications made with the anatase, another polymorph of TiO_2 - $Li_{0.5}TiO_2$ compound and a specific energy of 165 mAh/g have been obtained as a result of the reaction with lithium. A specific energy of 175 mAh/g has been obtained from the negative electrodes which were produced from $Li_4Ti_5O_{12}$ and Li_7Ti_5O12 compounds in the form of spinels. However, the cycle lives of both anatase and TiO_2 compounds in the form of spinel, were not as long as that of TiO_2

(B) in the form of nanotube [53].

TiO_2 (B) was first obtained by Marchand through the conversion of the hydrated compound belonging to $K_2Ti_4O_9$ and by calcining it at 500 ^oC. After calcination, a morphology in the form of a 3-dimensional nano-tube was obtained [54]. The structure obtained in the form of a nanotube, has more spaces than that of the rutile, anatase or brookite - it also has a continuous channel structure. Therefore, lithium-ions can easily enter into the nanotube structure during charge, and they can return without damaging the nanotube structure during discharge [55].

The silicon - whose theoretical specific capacity is approximately 4200 mAh/g - is one of the most important anode materials, and its theoretical capacity is approximately ten times greater than that of graphite-based anode materials [56]. The reaction of silicon - a negative electrode - with lithium results in $Li_{22}Si_5$ compound. The formation of this compound in the negative electrode, however, causes the electrode volume to increase by 400% [57]. The increase in the electrode volume causes high voltages in electrode. As a result of high voltages caused at the end of the cyclic loops, cracks and ultimately exfoliation occur on the negative electrode. This causes the capacity to be completely exhausted in a very short time [58].

In order to minimize the negative effects of the volumetric expansions, the studies have first focused on the accumulation of silicon on a nickel substrate. Because the silicon has a much higher affinity to oxygen than it does to nickel, a passivation layer has been formed on the nickel in the process of coating. The resulting passivation layer has served as a bond layer, ensuring the silicon to be better absorbed to the nickel surface. In the electrochemical studies carried out with 2C charge and discharge rate, a specific energy of 1700-2200 mAh/g was obtained after 750 cycles [59]. In order to remove the effects of volumetric expansion, studies were carried out on the production of negative electrodes from micron- and nano-sized powders. In the studies, micron- and nano-sized powders were dispersed in active/inactive matrices by using various binders, and thin silicon-based films were obtained. In particular, it has been observed that the negative electrodes produced from micron-sized silicon powders can quickly disintegrate and have very short cycle lives owing to the volumetric expansions [60]. Besides, the development of silicone-based nano composites has

shown that batteries resistant to volumetric expansion and with high specific battery capacity can be produced. The surface of the nano-sized silicon powders had been covered with a very thin carbon layer, and they were electrochemically charged and discharged between 0.02 and 1.2 V, at the rate of C/4. In the study, a specific energy of 700 mAh/g was obtained after 100 cycles [61]. In a similar study, after 100 cycles, a specific energy of 1000 mAh/g with the ratio of 0.3 mA/g was obtained from the electrochemical tests [62]. In the negative electrodes produced based on the nanocomposite idea, it has been observed that coating the silicon with carbon increases the structural stability and prevents the cracking and fragmentation resulting from volumetric expansion. Similarly, electrochemical treatments at 100 mAh/g to the negative electrodes obtained by coating the silicon in the nanosphere morphology with carbon have resulted in a specific capacity of 1450 mAh/g [58]. The electrochemical processes applied to the nanocomposites - which were obtained by coating them with silicon - at the rate of 250 mA/cm2 resulted in a specific capacity of 1000 mAh/g [58].

In recent years, particularly with the studies on silicon nanowires, it has been observed that after being exposed to a high level of expansion, negative electrodes were not exposed to any spillage and provided long service lives with high capacity values [56]. It has been stated that the theoretical battery capacity of the silicon thin films produced in the nanotube morphology was 75% after the initial discharge of 0.05 C and the decrease in the capacity was in the relative values. Silicon nanowires had been deposited on stainless steel substrates by using vapor-liquid-solid (VLS). Silicon nanowires approximately 89 nm in diameter had shown high resistance towards the volumetric expansion throughout the electrochemical tests. With the introduction of lithium-ions into the negative electrode, the diameter of the nanowire had risen approximately to 141 nm. Besides the volumetric expansion, the silicon nanowires which were crystalline in the beginning had been converted into amorphous Li_xSi compound. Similar amorphous conversions have been encountered in other studies [63]. The main reason why the high voltages resulting from volumetric expansion caused no damage to the electrode was that the distance between neighboring nanowires made it possible to tolerate the volumetric changes. As a result, it has been observed that the silicon-based anode materials produced in the form of nanowire were capable of maintaining

90% of their theoretical capacity after 100 cycles, as well as having 3 times more gravimetric capacity than that of carbons [64].

Tin oxide is one of the transparent semiconductors that provided one of the most important commercial developments. It has high optical transparency and high electrical conductivity - and these are some of its most important qualities for having a wide use area. Zinc oxide, indium oxide and titanium oxide, which have oxygen conductivity like tin oxide, can be used to achieve such desired properties. It is possible to encounter many studies on tin oxide among the literature examples [65]. In addition to this, there has been no study on the usage of tin oxide as the sole anode material in lithium-ion batteries.

Especially in the recent years, the use area of tin oxide thin films has considerably expanded. For example, tin oxide films, which are doped and undoped, are also intensively used while handling transparent conductive films [66], in architectural glass coatings due to their high reflectivity [67], and at the same time, as protective coating materials due to their high hardness as well as the chemical and mechanical stability [68]. Also, they are used in the identification of non-combustible gases and in solid-state gas sensors [69].

The tin oxide films can be produced by using a variety of techniques such as thermal evaporation [70], reactive sputtering [71], sol-gel techniques [72], chemical vapor deposition and spray pyrolysis [73]. The optical and electrical conductivity of these films depends mainly on the deposition technique.

When coated as a thin film layer, tin oxide has a high transparency up to 95%. Tin oxide is an n-type semi-conductor and is in the form of polycrystalline with an approximate optical band gap of 3.6 eV [74]. The properties of the tin oxide thin films vary depending on the method of preparation. For example, the microstructure of sputtered films may vary depending on the substrate and the deposition temperature. The film properties can also vary according to the temperature range, time and gas atmosphere. Tin oxide films are formed at low temperatures (<550 K) and in relatively amorphous and polycrystalline forms [70]. However, it has been observed in the literature that many crystal phases formed after the substrate were heated. Other factors affecting the film properties are the deposition rate of the condensed atoms

and the surface properties of the substrate.

The first testing of the tin metal as an electrode material in lithium-ion batteries was conducted by Foster et al. [75]. Later on, this study was developed further by Wen and Huggins [76]. When the studies of the three scientists are taken into consideration, it was observed that the binary lithium-tin system was made up of seven different phases, these were Li_2Sn_5, $LiSn$, Li_7Sn_3, Li_5Sn_2, $Li_{13}Sn_5$, Li_7Sn_2 and $Li_{22}Sn_5$. Later on, as a result of Courtney's study, the diagram of lithium-tin phase and voltage curve of lithium-tin compound were developed [77]. It has been proven by subsequent studies that the theoretical results were consistent with the experimental studies [78].

The tin-based material with the highest capacity among the anode materials used in lithium-ion batteries is tin oxide (1497 $mAhg^{-1}$) [79]. Especially after obtaining high yields from tin-based amorphous oxide materials, there is a growing interest in the use of tin oxide as a negative electrode [80]. The first tin oxide-based lithium-ion battery was commercially released by Fuji in 1995 [80]. The amount of specific energy obtained from the electrode material that was made up of tin-based glass compounds had been higher than 600 $mAhgr^{-1}$. Following the successful commercial applications of tin-based electrode materials, the interest in tin and tin alloys has increased more. In-situ X-ray characterizations, especially during electrochemical processes, have also been studied in detail for their reactions with different lithium-tin compounds [81]. In the studies carried out until now, what the compounds that have been obtained as a result of the reaction of tin-based compounds - particularly such as SnO, SnO_2, SnP_2O_7, $SnHPO_4$, $SnPO_4Cl$, $SnSiO_3$, $SnBPO_6$, $Sn(C_2O_4)$ and $SnSO_4$ - with lithium, are not precisely known [82].

The first tin-based electrode material that was tested after Fuji's tin oxide-based lithium-ion battery patent was SnO [81]. It has been observed that the reaction of the SnO compound - which has a layered structure - with lithium is complicated and comprised of many steps. Besides LiO_2 formation, one of the main reasons is the reduction of Sn(II) to Sn(0). In the studies, a specific energy density of approximately 600 $mAhg^{-1}$was obtained after the complete reduction of the tin metal [82].

1.2.3 Electrolyte Materials

Another important factor while evaluating the performance of lithium-ion cells is electrolytes. Due to active nature of lithium, organic electrolyte systems should be used in lithium-ion batteries. The electrolyte component is made up of salts or anions mostly dissolved in an organic solvent. Non-liquid electrolytes also continue to be intensively studied today. Today, liquid polymer electrolytes are also used as electrolyte materials in secondary lithium-ion batteries. Lithium-ion polymer and lithium polymer batteries are being commercially produced. A number of glasses and ceramics capable of conducting lithium-ions can also be used as solid-state electrolyte materials in lithium-ion batteries. Besides being too complicated, liquid electrolyte systems for lithium-ion batteries are used in a certain combination of lithium salts and organic solvents. In addition to being non-toxic, lithium salts should also be thermally, chemically or electrochemically stable. In addition to these qualities, electrolyte materials should have high solubility, ion conductivity and be able work with all cell elements. The most intensively used lithium salts can be listed as $LiClO_4$, $LiAsF_6$, $LiPF_6$, $LiSO_3CF_3$ and $LiN(SO_2CF)_3$. These salts have brought about a number of problems. The fact that $LiClO_4$ is thermally unstable and has explosion risk can be given as an example. Besides being unstable in solid-state, $LiPF_6$ salt has a tendency of producing LiF and PF_5 (Lewis) acid when added to solution [83].

The most popular solvents used in obtaining electrolytes are Polypropylene Carbonate (PC), 1,2-dimethyloxyethane (DMC), ethylene carbonate (EC), diethyl carbonate (DEC), tetrahydrofuran (THF) and 2-methyltetrahydrofuran (2MeTHF). As mentioned before, the formation of a passivation film on the surface of the carbon is very important for a lithium-ion battery which contains carbon anode to operate successfully. The solvents used in lithium-ion battery systems should be stable (organic or inorganic) and able to form lithium salts that can passivate the surface of the anode [84].

Most of the conductive polymers were developed in the last two decades. The polymer electrolytes were developed thanks to the co-operation of various disciplines such as electrochemistry, polymer science, organic chemistry and inorganic chemistry. One of the most important applications areas of polymer electrodes is their use

as solid-state electrolytes in lithium and lithium-ion batteries. It is an important issue that solid polymers capable of conducting lithium-ions must meet a number of criteria:

1. Ionic Conductivity: The ionic conductivity of a solid polymer electrolyte should be at least 70% of the ionic conductivity of liquid electrolytes. Accordingly, the charge and use of the batteries can be provided at different current densities [85].

2. Chemical, Thermal, Electrochemical Stability: The polymer electrolyte should be chemically inert with anode and cathode. In order for the batteries to work, they must have chemical stability between 0 and 4.5 V. Plus, the polymer electrolyte has to be highly resistant towards high temperatures. This is because, depending on the operating conditions, the temperature can occasionally rise in the devices they are used [86].

3. Mechanical Strength: At the same time, polymer electrolyte should serve as a separator inside the battery. The nonoccurrence of a short-circuit between anode and cathode depends on the mechanical strength of the polymer.

There are two polymer electrolyte systems available today. These can be listed as pure solid polymer electrolyte and gel polymer electrolyte systems. While generally showing low ionic conductivity, solid polymer electrolytes also have a high mechanical strength. On the contrary, gelatinous polymer electrolytes possess a high ionic conductivity and a low mechanical strength. Polymeric electrolytes are prepared by using polymers such as polyvinylidene fluoride (PVdF), polymethyl methacrylate (PMMA) and polyacrylonitrile (PAN), along with various lithium salts (X = $(PF_6)^{-1}$, $(ClO_4)^{-1}$, $(BF_4)^{-1}$, $N(CF_3SO_2)_2$). The gel structure can be obtained either by using chemical methods or by mechanically obtaining the cross-link formation. The polymeric electrolytes, in lithium-ion batteries that are used today, are preferred because of both their Li-ion conductivity and flexibility [87].

1.3 Problems of Anode Materials in Li-ion Batteries

Ideal anode material for lithium ion batteries is lithium. However, dentritic formation of lithium on the surface of the contact during charging causes shortcut between anode and cathode by-passing the separator. Because of this instability of the anode material, researchers try to find efficient replacement of lithium. Better yet, they found suitable replacement to electrolyte (reported as found by Qian et.al. [88]) which would not let lithium to form dendrites.

Anode material of the commercial batteries is graphite. Li intercalates to the layered structure of carbon in this system. However, theoretical charge capacity of carbon is lower compared to metals. In those metallic systems, storing lithium can be achieved by alloying. The process is called lithiation. Counter-reaction is called delithiation which lithium ions leave negative electrode and migrates to positive electrode. Li is very active material and it can alloy various metal elements such as Mg, Ca, Al, Si, Ge, Sn, Pb, As, Sb, Bi, Pt, Ag, Au, Zn, Cd, Hg, etc. [89]. Although the high variety, high efficiency and high abundance of those metal elements, the reasons behind not to use any metal as anode material in Li-ion batteries are due to both chemical and mechanical instability of those materials [90]. Major drawback is, during lithiation-delithiation processes of electrode material, mechanical integrity is damaged caused by volume change. In Li-C system, host(carbon) does not change its structure, considerably. Volume change is minimum. For metals which form intermetallic compounds with lithium, volume change is so large that structure of the battery is damaged. This structural defective mechanism is called pulverization and it shows itself in cyclability as a rapid decrease of charge capacity over cycles.

For that, nanostructured materials are proposed. However, materials in nanoscale have very large surface area and as a consequence of that, during cycling, probability of joining and merging those porous structure into bulk material increases. This causes a minor problem. To preserve the structure, application of nanostructured active material in an inert matrix is proposed. When Tin (IV) Oxide is used as nanostructured anode material, inert LiO_2 coating is formed itself during lithiation. This

inert matrix conserve the initial structure. The equation follows,

$$SnO_2 + 4Li \longrightarrow Sn + 2Li_2O \tag{1.3}$$

This reaction is not reversible and causes capacity loss due to inactive lithium component, LiO_2. For metal oxide anode materials, oxygen form lithium oxide during lithiation and it does not decompose in the delithiation process. This phenomena is called irreversible reactions problem and to solve this problem, researchers try to alloy the active materials.

Highest charge capacity among alternative materials to graphite is silicon. Tin and aluminum are the second. Silicon was attractive to the companies due to huge charge capacity. Therefore researches are funded, exceedingly.

Aluminum is attractive to the military projects due to its thermal properties. High temperature thermal batteries researches are funded by military in the USA.

Tin was the third option, so far. Lately, researches about tin alloys are in demand due to indiscoverable variety of electrochemical properties of those. Tin oxide is the terminus a quo of tin alloys since it is processable in nanoscale.

1.3.1 Solutions

1.3.1.1 Nanostructured Materials

Nanostructured materials are used as anode material to eliminate the pulverization problem. Electrodes, compose of hollow spheres or 2D nanostructures, have porous structure such that very small nano or micro scale pores distributed homogenously over the all body of the electrodes. This property allows electrodes to expand inside those pores instead outsider expansion of the bulk electrode. This helps to eliminate pulverization problem as in figure 1.2.

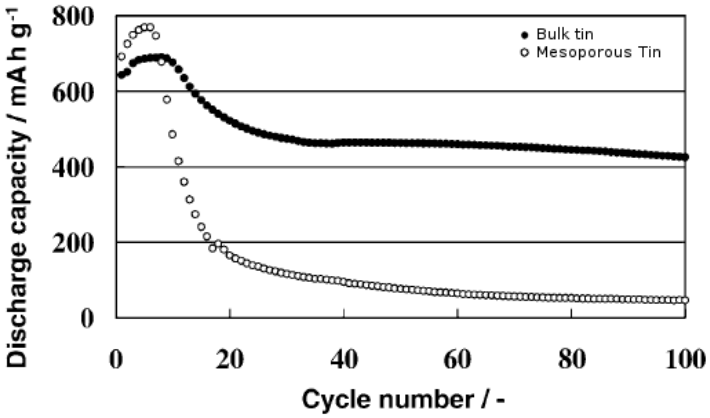


Figure 1.2: Effect of the morphology [3]. Bulk tin is presented with hollow points and mesoporous tin material is presented with solid points.

Decreasing the particle size to nano-scale, increaseas cyclability dramatically according to figure 1.3.

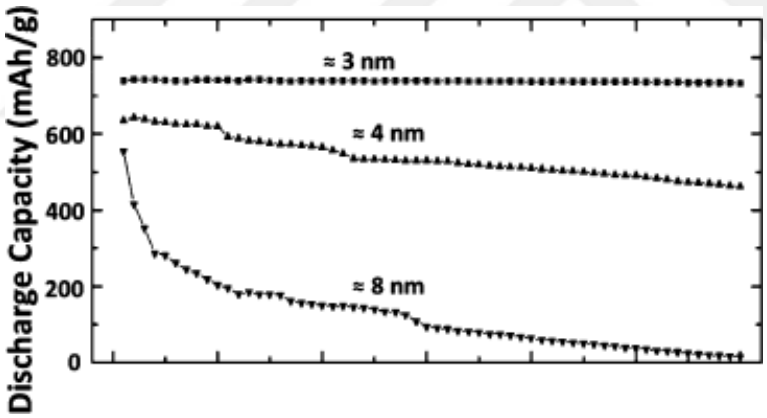


Figure 1.3: Effect of particle size [3].

There are two methods for nanoscale powder production, sol-gel and hydrothermal methods. It is well-known that hydrothermal method is a more efficient way for controlling particle size of the product. The basic two parameters in the hydrothermal method are temperature and time.

Fujihara and his colleagues [91], compared the powder sizes produced by hydrother-

mal method with varying temperature and keeping the processing time constant. They used $SnCl_4.5H_2O$ as the precursor. Time was constant, 24 hours. Temperature is varied between 100 and 200 °C. The relationship between temperature and particle size is given in the table 1.2. Particle size is increased with the temperature as expected. However, it is seen that for surface area, there must be an optimum temperature.

Table 1.2: Influence to the particle size of the temperature in the aqueous solution treated for 24 hours.

Temperature	**Particle Size**(nm)	**Surface Area**(m^2/g)	**Pore Size** (nm)
100	4.5	218	<2.7
150	5.4	225	3.9
200	6	209	3.8

Another study by Chen et al., they kept temperature constant and vary the time between 6 and 24 hours. They used tin folio as the precursor and NaOH to control the pH value of the solution. SEM images of the products are in figure 1.4.

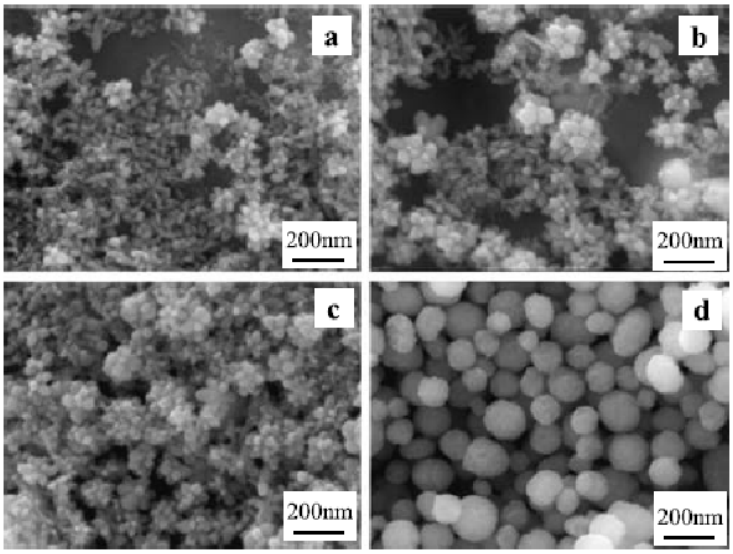


Figure 1.4: SEM images of the products treated for 6(a), 12(b), 18(c) and 24(d) hours at 180 °C.

This study shows how tin oxide spheres are formed. In first six hours nanoparticles were formed. Those aggreageted particles have became nucleation sites for tin oxide spheres. Those spheres have became bigger and smoother after 24 hours.

Other studies show that morphology of the product is not only sphere, also flowers and plates. In the study of Yin et al. [92], they managed to produce hierarchical form of tin oxide plates as flowers. They used tin sulfate as the precursor. The solution is treated at 120 ^{o}C for 48 hours. They claim that SO_4 compund in the precursor lower the pH value and spheres could not form. Instead plates are formed. pH value must have affected the surface energy of the facets.

Different structures were, also, formed by using different surfactants. Rajendran et al. studied with anionic(SDS), cationic(CTAB) and unionic(PEG) surfactants and compare the products as in figure 1.3.

Table 1.3: Shape and dimensions of tin oxide structures prepared with different surfactants.

Surfactant	**Particle Size**(nm)	**Surface Area**(m^2/g)	**Structure**
SDS	8	112.10	Flower
CTAB	11	81.53	Cauliflower
PEG	13	68.98	Plates

1.3.1.2 Alloying with Active Materials

For instance, Sn-Sb alloy is used by Wang et.al. [93]. They used hydrogen plasma-metal reaction to produce spherical shaped Sn-Sb alloy nanoscale powders. They measured cycling performances of different compositions and they found that $Sn-46.5at\%Sb$ alloy started with capacity of $701mAhg^{-1}$ which is lower than the theoretical capacity of pure tin, higher than pure antimony, as composite theory dictates. However, after 20 cycles, charge capacity of $Sn-46.5at\%Sb$ alloy decreases to $566mAhg^{-1}$ and remained there which is much higher than pure tin after 20 cycles($220mAhg^{-1}$ [90].). They used the stability of antimony and high charge capacity of tin to produce advance composite material.

Not all composite materials obey composite theory. In the study of Rahman et. al. [94], they propose a system consists of Fe_2O_3, Tin (IV) Oxide and C which has much higher charge capacity than its components(Fe_2O_3-Tin (IV) Oxide-C system has charge capacity of $1110mAhg^{-1}$, the components have $1007mAhg^{-1}$ [94], $780mAhg^{-1}$ and $373.8mAhg^{-1}$, respectively.). To explain this phenomena, they

suggested that the system alters the irreversible reactions as reversible ones. Tin (IV) Oxide itself reacts with lithium as,

$$SnO_2 + 4Li \longrightarrow Sn + 2Li_2O \tag{1.4}$$

Fe_2O_3 reacts as,

$$Fe_2O_3 + 6Li \longleftrightarrow 2Fe + 3Li_2O \tag{1.5}$$

Since Fe^{3+} ion can reduce Li_2O, lost charges by Tin (IV) Oxide are retrieved by Fe_2O_3, other active component in the system. However, according to Guo et. al. [95], with effect of C, the equation 1.4 may become,

$$SnO + 2Li \longleftrightarrow Sn + Li_2O \tag{1.6}$$

In that case, they suggested that the carbon element coordinated with Tin (II) Oxide alters the irreversible reactions.

Alloying with another metals are promising, also. For example, effect of alloying with cobalt is studied and became commercially available by Sony. 18650 Nexelion Sony battery utilizes a tin compound as an anode material and offer higher charge capacity than graphite and offer stability, figure 1.5.

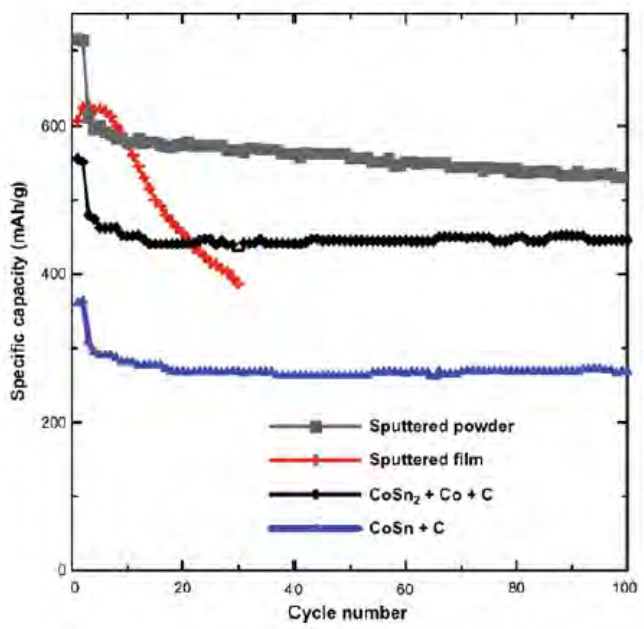


Figure 1.5: Effect of alloying with cobalt [3], 18650 Nexelion Sony battery. Sputtered powder and sputtered film curves are irrelevant. Alloyed tin curves show stability and cyclability unlike pure tin and tin oxides.

1.4 Hydrothermal Treatment and Formation of Tin Oxides

According to Chen et. al. [96], it is difficult to produce pure Tin (IV) Oxide due to challenges in variations of oxidation states of tin (II) ions to tin (IV) ions. They used $SnCl_2.2H_2O$ to produce flower-like structures made out by nanosheets. They, also, suggested reaction mechanism for that is,

$$6Sn^{2+} + 8H_2O \longrightarrow Sn_6O_4(OH)_4 + 12H^+ \tag{1.7}$$

$$Sn_6O_4(OH)_4 + 3O_2 \longrightarrow 6SnO_2 + 2H_2O \tag{1.8}$$

The mechanism involves $Sn_6O_4(OH)_4$ intermediate compound and they claim that $Sn_6O_4(OH)_4$ compound have important role in the mechanism. Using tin (IV) salts, Tin (IV) Oxide nanosheets cannot be produced without any surfactant or chemical agent because of the formation of $Sn(OH)_4$ compound. When tin (IV) salts are used agglomerated nano or micro scaled particles are produced.

Parallel to that theory, in the study of Zhu et. al. [97], they produce Tin (IV) Oxide nanoparticles so called quantum dots, with precursor of $SnCl_4.5H_2O$. As additive materials, they try $NaOH$ and $N_2H_4.H_2O$. For both materials, they suggested a reaction mechanisms for producing Tin (IV) Oxide quantum dots. That are, For $NaOH$:

$$SnCl_4 + 4NaOH \longrightarrow Sn(OH)_4 + 4NaCl \tag{1.9}$$

$$Sn(OH)_4 \longrightarrow SnO_2 + 2H_2O \tag{1.10}$$

Equation 1.9 occurs before hydrothermal process, and equation 1.10 during the process.

For $N_2H_4.2H_2O$:

$$mSnCl_4 + nN_2H_4 \longrightarrow (SnCl_4)_m(N_2H_4)_n \tag{1.11}$$

$$(SnCl_4)_m(N_2H_4)_n \longrightarrow mSn^{4+} + nN_2H_4 + 4mCl^- \tag{1.12}$$

$$3N_2H_4 + 4H_2O \longrightarrow 4NH_4OH + N_2 \tag{1.13}$$

$$Sn^{4+} + 4NH_4OH \longrightarrow SnO_2 + 4NH_4^+ + 2H_2O \tag{1.14}$$

Equation 1.11 and 1.12 before hydrothermal process, equation 1.13 and 1.14 during process.

Similar results are reported by Wu et. al. [98], using amino acids as additive materials.

There are three approaches to kinetics of Tin (IV) Oxide formation in the process of hydrothermal treatment. One of them, (the study of Shao et. al. [99], as introduced in section **??**), Tin (IV) Oxide hollow spheres are formed in alkaline media. Since high pH value leads rapidly forming and growing Tin (IV) Oxide crystals, they create depleted region for Sn^{+4} ions. While they grow, they surround the depleted region and seal it.

Another approach by Yin et. al. [100], similar to the first one, they found that formation of Tin (IV) Oxide structures follows four steps according to the results of their

study which they conducted time dependent experiments for 20 min, 1 hour, 24 hours and 48 hours of hydrothermal treatments at 393K using $SnSO_4$ as precursor in water solution. According to results, formation of Tin (IV) Oxide structures is kinetically controlled Ostwald ripening process as indicated in the study, and the steps are:

Step 1: Oxidation and hydrolysis of tin ions results in an aggregated (with low diffraction intensity) amorphous or poor crystallized phase. Those aggregated masses are initial core material for the resulted powder.

Step 2: Then Tin (IV) Oxide nanosheets form on the spheres while composition of tin ions decreases.

Step 3: These nanosheets becomes nucleation sites for more nanosheets.

Step 4: Finally the nanosheets form hollow Tin (IV) Oxide spheres-like hierarchical structures(with high diffraction intensity) by consuming initial core material (Ostwald Ripening process).

The process can be summarized as formation of hollow spheres by consuming agglomerated Tin (IV) Oxide nanocrystals. In most literature, this process is attributed to Ostwald ripening process [100–108], however, there is another study which specially addresses to formation of Tin (IV) Oxide nanocrystals by Lee et. al. [109]. They claim that the formation process of Tin (IV) Oxide nanocrystals is oriented attachment process. The nanoparticles in Brownian motion collides and they either collide in same crystallographic alignment then coalescence occurs or they do not collide in same alignment then they repel each other.

Overall, the formation of Tin (IV) Oxide might be attributed to a process which started with oriented attachment then Ostwald ripening to form final structure.

Soufyane et. al. [110], in their experiments, showed that changing only composition results in the product as Tin (II) Oxide or Tin (IV) Oxide. 2g $SnCl_2.2H_2O$ or 1g $SnCl_2.2H_2O$ dissolved in 0.35M $NaOH$ solution and, after hydrothermal treatment, Tin (II) Oxide or Tin (IV) Oxide is produced, respectively. The article gave no information about yield.

Several chemicals can be used to control pH values. We used NH_4OH, however,

KOH, $N_2H_4.H_2O$, NaOH and others are also used in literature. One study by Zhu et. al [111]., compare KOH and $N_2H_4.H_2O$. According to them, $N_2H_4.H_2O$ while adjusting pH value, it also prevent further oxidation of Tin (II) Oxide microsheets to Tin (IV) Oxide. When they use KOH under same conditions they collected the product as a phase mixture of Tin (II) Oxide and Tin (IV) Oxide. Another study uses NaOH by Khuc et. al. [112], their experiments are resulted in formation of Tin (IV) Oxide nanorods. It must be noted that their experiments are done at high pH values. They suggest a mechanism that involves CTAB as a surfactant, but Qin et. al. [113], proposed that using only NaOH with ethanol present, Tin (IV) Oxide nanorods can be produced. Common in both studies that NaOH is not only an additive to adjust pH value, but also a morphological factor. Both studies suggest that $Sn(OH)_6^{2-}$ or $Na_2Sn(OH)_6$ is important intermediate compound which can be exist when NaOH is used. The reaction mechanism follows [113],

$$SnCl_4 + 6NaOH \longrightarrow Na_2Sn(OH)_6 + 4NaCl \tag{1.15}$$

$$Na_2Sn(OH)_6 \longrightarrow SnO_2 + 2NaOH + 2H_2O \tag{1.16}$$

Another explanation to the effect of the additive material to adjust pH value, comes from crystallographic approach. Birkel et. al. [114], in their studies based on interaction of alkaline metal cations to oxidic surfaces using molecular dynamics program, found that NH_3^+ compound has smaller adsorption energy on the (110) surface, than Na^+ compound($Na^+ > K^+ > Rb^+ > Cs^+ > TMAH > NH_3$). That plane is relatively more important due to being the most stable plane in Tin (IV) Oxide structure. The order of energies of the planes is (110) < (100) < (101) < (001). As a consequence of that, it is also suggested by Sato et. al. [108], preferable growth direction of the Tin (IV) Oxide structure is [001] direction.

Growth direction changes from [001] to [101] when HCl is used to lower the pH value in ethanol based solution. In the study of Wang et. al. [115], they used $SnCl_2.2H_2O$ in 30ml non-aqueous ethanol solution added 0.9ml 37% HCl processed for 12 hours at 200 ^oC and they collected 150nm flower-like hierarchical micro spheres made out of nanorods, which they preferentially growth in the direction of [101].

Experimental results of the study done by Liu et. al. [116], shows that hydrothermally

treated products at 180 °C shows better thermal stability against crystal growth during heat treatment that of hydrothermally treated at 170 °C. The cause which induces variation on the stability, might also change other properties of the product.

CHAPTER 2

EXPERIMENTAL PROCEDURE

In this study, phase pure or alloyed tin monoxide and tin dioxide were produced as anode materials for Li-ion batteries using hydrothermal treatment. Concentration of the raw material, time and pH value and composition of the solution were the main parameters as alloying elements La, W, Y and Zr.

2.1 Hydrothermal Processing of Materials

71.4mM of tin-based solution was prepared by mixing 1050 ml deionized water, 350 ml ethanol (If water and ethanol proportion was three to one, Wtr:EtOH=3:1. Total volume of the solution was 1400 ml.) and 0.1 moles $SnCl_2.2H_2O$ (22.5 g) in that order at room temperature. If concentration of tin ions was 0.01 moles(C=0.01 moles or 7.14 mM, 2.26 g of the precursor was used.). After solution was mixed rapidly, pH value is close to 1.8. If concentration of tin ions was 7.14 or 3.57 mM, pH value was close to 2.4 and 2.9, respectively. Then, pH value was fixed to desired values by adding NH_4OH or HCl solution. The solution was hydrothermally treated at 200 ^oC or 180 ^oC for 3, 12 or 24 hours. After hydrothermal stage, the solution was cooled down to nearly room temperature in the system. Subsequently, it was washed with deionized water, and dried in air.

Parameters of chosen experimental procedure for Tin (IV) Oxide and Tin (II) Oxide were given in the table 3.3. Same experimental procedures handled for alloying process. Before hydrothermal stage during preparing solution, solvent was added to the container contains $1-x$ moles $SnCl_2.2H_2O$ and x moles alloying salts(x=0.05).

It was observed that the powders are not reacting on contact. Alloying salts were added to solution in x over $1-x$ proportions were Lanthanum(III) nitrate hexahydrate ($La(NO_3)_3.6H_2O$), Yttrium(III) nitrate hexahydrate ($Y(NO_3)_3.6H_2O$), Ammonium meta-tungstate hydrate ($(NH_4)_6H_2W_{12}O_{40}.xH_2O$), zirconium(IV) oxynitrate hydrate ($ZrO(NO_3)_2.xH_2O$).

As an oxidation agent $K_2S_2O_8$ was also used. Similarly, solution was prepared with 0.1 moles $SnCl_2.2H_2O$ and 1400 ml deionized water. Ethanol was not used in the solution. After solution was prepared, to adjust pH value, ammonia solution was used. Finally, $K_2S_2O_8$ was added with a molar ratio of 1:1 or 4:1 as $K_2S_2O_8$:$SnCl_2.2H_2O$. The temperature was reached 120 ^oC in one hour during hydrothermal process, subsequently the temperature was held at 120 ^oC for 280 minutes.

Naming of specimens and experimental parameters were given in the following tables.

Table 2.1: Experiments: Concentration is less than 0.1 moles. 'T','t','C', refers to temperature, time, concentration in moles of Sn, respectively.

Code	**T(^oC)**	**t(h)**	**starting pH**	**Wtr:EtOH**	**C**
Sn005ph29	200	3	2.9	1:0	0.005
Sn005ph90	200	3	9	1:0	0.005
Sn005ph103	200	3	10.3	1:0	0.005
Sn01pH24	200	3	2.4	3:1	0.01
Sn01pH24t12	200	12	2.4	3:1	0.01
Sn01pH88	200	3	8.8	3:1	0.01
Sn01pH105	200	3	10.5	3:1	0.01

Table 2.2: Experiments: Concentration is 0.1 moles, water-ethanol mixture higher than or equal to three to one.

Code	**T(°C)**	**t(h)**	**starting pH**	**Wtr:EtOH**	**C**
SnWaterpH21	200	3	2.1	1:0	0.1
SnWaterpH30	200	3	3	1:0	0.1
SnWaterpH86	200	3	8.6	1:0	0.1
SnWaterpH95	200	3	9.5	1:0	0.1
SnWaterpH101	200	3	10.1	1:0	0.1
Sn19ph009	200	3	0.9	3:1	0.1
Sn19ph14	200	3	1.4	3:1	0.1
Sn20ph14	200	3	1.4	3:1	0.1
Sn19ph19	200	3	1.9	3:1	0.1
Sn20ph18	200	12	1.8	3:1	0.1
Sn19ph30	200	3	3.1	3:1	0.1
Sn21ph80	200	3	8	3:1	0.1
Sn22ph76	200	12	7.6	3:1	0.1
Sn23ph93	200	3	9.3	3:1	0.1
Sn23NaOHph125	200	3	12.5	3:1	0.1

Table 2.3: Experiments: Concentration is 0.1 moles, water-ethanol mixture lower than three to one.

Code	**T(°C)**	**t(h)**	**starting pH**	**Wtr:EtOH**	**C**
Sn13ph19	200	3	1.9	1:3	0.1
Sn15ph78	200	3	7.8	1:3	0.1
SnEtOHph17	200	3	1.7	0:1	0.1

Table 2.4: Experiments: Chosen experimental procedure for Tin (IV) Oxide and Tin (II) Oxide.

Code	**T(°C)**	**t(h)**	**starting pH**	**Wtr:EtOH**	**C**
Sn66ph57	180	4	5.7	5:1	0.1
Sn112ph19	200	24	1.9	1:1	0.1

Table 2.5: Experiments of alloying tin oxide with La, Y, W and Zr.

Code	**T(°C)**	**t(h)**	**starting pH**	**Wtr:EtOH**	**C**
SnO2La19ph21	200	24	2.1	1:1	0.1
SnOLa19pH65	180	4	6.5	5:1	0.1
SnOLa19pH75	180	4	7.5	5:1	0.1
SnOLa19pH87	180	4	8.7	5:1	0.1
SnOLa19pH91	180	4	9.1	5:1	0.1
SnO2Y19pH22	200	24	2.2	1:1	0.1
SnOY19pH75X(a)	180	4	7.5	5:1	0.1
SnO2W19pH21(a)	200	24	2.1	1:1	0.1
SnOW19pH80(a)	180	4	8.0	5:1	0.1
SnO2Zr19pH19	200	24	1.9	1:1	0.1
SnOZr19pH80	180	4	8.0	5:1	0.1

Table 2.6: Parameters and XRD test results of experiments on tin oxide production using $K_2S_2O_8$ as oxidation agent. (Abbreviation is used, T is for the temperature)

Code	**T(°C)**	**ratio**	**starting pH**
SnK2S2O8pH12	RT	1:4	1.25
SnK2S2O8EpH09	RT	1:1	0.9
SnK2S2O8pH94	RT	1:4	9.45
SnK2S2O8EpH101	RT	1:1	10.1

2.2 Crystallographic and Morphological Characterization

SEM images were taken by "FEI 430 Nano Scanning Electron Microscope" (SEM) equipped with an energy dispersive Xray spectroscopy (EDS) analyze and HRTEM images were taken by Jeol JEM2100F Field Emission Transmission Electron Microscope. XRD characterizations of the product were made by X-ray diffractometer "Rigaku D/Max 2200" (Cu-Kα radiation operating at 40kV) by continuous scanning between 10^o and 90^o 2Θ angles with a scan speed of $2^o/\mathrm{min}$ and Rietveld analysis were made by a software program, MAUD.

Crystallographic data of Tin (IV) Oxide(Cassiterite, JCPDS file No. 41-1445) and Tin (II) Oxide(Romarchite, JCPDS file No. 06-395) are space groups of P42/mnm and P4/nmm:2 tetragonal latices, respectively. Their lattice parameters a and c are 4.7397 and 3.1877 angstroms for Tin (IV) Oxide, 3.7986 and 4.8408 angstroms for Tin (II) Oxide.

2.3 Electrode Fabrication and Measurements

In a typical measurement experiment to fabricate electrodes, active material (Tin (II) Oxide, Tin (IV) Oxide or doped materials), carbon black and and PVDF as binder are mixed in mass ratio of 7:2:10. Obtained slurry was coated on Cu foil. After drying at 120 ^{o}C for one day under vacuum, 18mm electrodes were cut and put into glovebox. Cells were assembled using lithium metal as counter electrode and 1M $LiPF_6$ solution of mixture of EC and DEC in equal weight as electrolyte. Galvanic cycling measurements were done at 0.5mA, 1mA and 1.5mA current.

CHAPTER 3

RESULTS AND DISCUSSION

3.1 Qualitative Analysis of the Products

Powders produced by hydrothermal treatment was achieved successfully. Production methods for producing phase pure SnO and SnO_2 were optimized. Both of the materials are considered as different anode material.

3.2 Quantative Phase and Yield Analysis of the Products

Quantitative analysis and results of the experiments were given as yield, phase percentages and texture in the tables below.

Table 3.1: Results: Concentration is less than 0.1 moles.

Product		SnO		SnO_2	
Code	**Yield(g)**	**%**	**Texture**	**%**	**Texture**
Sn005ph29	0.4	0	-	100	-
Sn005ph90	0.41	47.9	(001)	52.1	-
Sn005ph103	0.55	36.7	(001)	63.3	-
Sn01pH24	0.66	0.3	-	99.7	-
Sn01pH24t12	0.76	0.2	-	99.8	(110)
Sn01pH88	1.10	6.2	(101)	93.8	-
Sn01pH105	1.25	10.9	(101)	89.1	-

Table 3.2: Results: Concentration is 0.1 moles, water-ethanol mixture lower than three to one.

Product		SnO		SnO_2	
Code	**Yield(g)**	**%**	**Texture**	**%**	**Texture**
Sn13ph19	2.97	8.4	-	91.6	-
Sn15ph78	11.28	61.8	(001)	38.2	-
SnEtOHph17	3.7	7.3	-	92.7	-

Table 3.3: Results: Chosen experimental procedure for Tin (IV) Oxide and Tin (II) Oxide.

Product		SnO		SnO_2	
Code	**Yield(g)**	**%**	**Texture**	**%**	**Texture**
Sn66ph57	12.85	97.3	(001)	2.7	-
Sn112ph19	2.45	0.6	-	99.4	-

Table 3.4: Results: Concentration is 0.1 moles, water-ethanol mixture higher than or equal to three to one.

Product		SnO		SnO_2	
Code	**Yield(g)**	**%**	**Texture**	**%**	**Texture**
SnWaterpH21	0.5	10	(001)	90	-
SnWaterpH30	10.5	95.6	(001)	4.4	-
SnWaterpH86	13.2	96.1	(001)	3.9	-
SnWaterpH95	13.1	94.1	(001)	5.9	-
SnWaterpH101	12.8	94.2	(001)	5.8	-
Sn19ph009	0.33	5.4	-	95.6	-
Sn19ph14	1.24	0.8	-	99.2	-
Sn20ph14	0.62	0.7	-	99.3	-
Sn19ph19	1.29	1.3	-	98.7	-
Sn20ph18	1.18			100	-
Sn19ph30	8.24	45.2	(001)	54.8	-
Sn21ph80	11.92	95.7	(001)	4.3	-
Sn22ph76	13.04	73.9	-	26.1	-
Sn23ph93	12.45	95.3	-	4.7	-
Sn23NaOHph125	1.16	29.7	(001)	70.3	-

Table 3.5: Results of alloying tin oxide with La, Y, W and Zr.

Product		SnO		SnO_2	
Code	**Yield(g)**	**%**	**Texture**	**%**	**Texture**
SnO2La19ph21	3.71	0	-	100	(110)
SnOLa19pH65	13.24	55.8	(001)	44.2	-
SnOLa19pH75	13.58	30.6	(001)	69.4	-
SnOLa19pH87	13.34	45.4	(001)	54.6	-
SnOLa19pH91	14.60	51.7	-	48.3	-
SnO2Y19pH22	6.7	0.4	-	99.6	(110)
SnOY19pH75X(a)	12.95	-	-	-	-
SnO2W19pH21(a)	2.7	-	-	-	-
SnOW19pH80(a)	13.57	-	-	-	-
SnO2Zr19pH19	3.8	0	-	(100)	-
SnOZr19pH80	13.0	76.1	(001)	23.9	-

Table 3.6: XRD test results of experiments on tin oxide production using $K_2S_2O_8$ as oxidation agent.

Product		SnO		SnO_2	
Code	**Yield**	**%**	**Texture**	**%**	**Texture**
SnK2S2O8pH12	6.9	10.2	-	89.8	-
SnK2S2O8EpH09	18.33	1.3	-	98.7	-
SnK2S2O8pH94	13.2	22.8	-	77.2	-
SnK2S2O8EpH101	11.5	9.3	-	90.7	-

3.3 Crystallographic and Morphological Characterization

3.3.1 Effects of Processing Time and Concentration

3.3.1.1 Morphology

The results of experiments Sn01pH24 and Sn01pH24t12 are parallel to that theory of Yin et. al. [100]. According to the results, the phase does not exhibit high intense peaks up to 48 hours 120 °C. Our experiments show that increasing in time, resulted with higher degree of crystallization (See figure 3.1). They, also, inform us that, for Tin (IV) Oxide, (110) plane is the preferred orientation which was confirmed by XRD analysis of Sn01pH24t12. Their solution contained near 5mM tin ions and our solution for Sn001 series were 7.14mM of tin ions close to that value.

However, in our experiments hydrothermal treatment conducted at 200 °C, therefore crystallization of aggregated spheres expected in less time. When the concentration increases to 71.4mM in our experiments, even hydrothermal treatment of 12 hours is not enough for crystallization of Tin (IV) Oxide as in SnWaterpH21, or perhaps higher temperature is required.

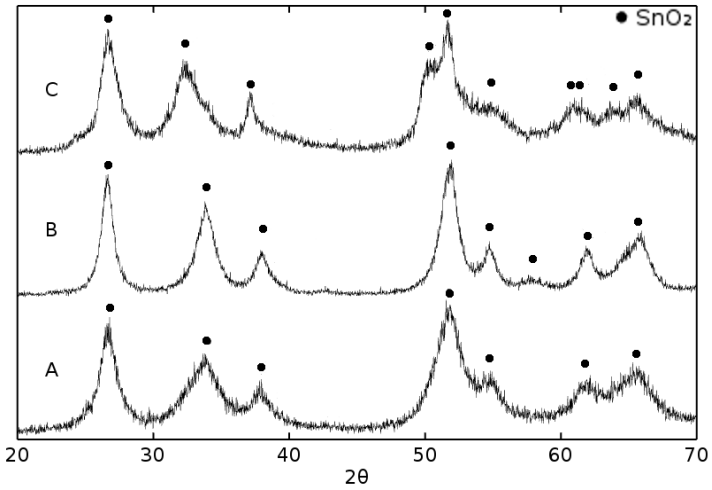


Figure 3.1: XRD diagrams of Sn01pH24(A) and Sn01pH24t12(B). Same solution is prepared for A(Sn01pH24) and B(Sn01pH24t12), concentration of tin ions in the solution of C(SnWaterpH21) is ten times higher concentrated. Hydrothermal treatments are prolonged 3 hours for Sn01pH24 and SnWaterpH21, 12 hours for Sn01pH24t12.

These show that, production of Tin (IV) Oxide is a kinetically controlled process, as it is mentioned in the introduction, by both time and concentration. Increasing in concentration might retard the process. However, according to Lou et. al. [102], changing concentration, also, effects the morphology of the product. To test this theory, we need to experiment with high concentration in a sufficiently long time of hydrothermal treatment, because it might be argued that our experiments with concentration of 71.4mM corresponds to only early steps of the process explained earlier in this section.

3.3.1.2 Dominant Phase

Beside morphology, time is also important for the composition of different oxide phases, if we look at the XRD test results. Since it is related to formation of Tin (II) Oxide phase, this will be discussed at section 3.3.2.

Changing concentration affects the dominant phase of the product [110]. This phenomena is also observed in our study. Our study indicates that increasing in the concentration increases the Tin (II) Oxide, lower the Tin (IV) Oxide composition in the product for limited time of hydrothermal treatment (See figure 3.2).

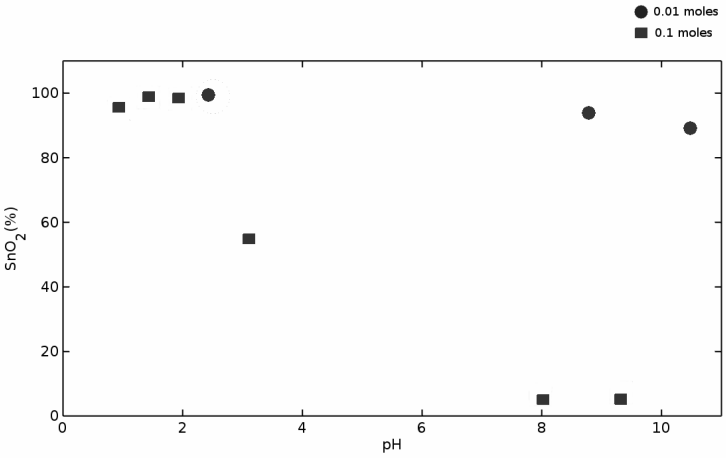


Figure 3.2: Dependence of the composition of the phases on concentration of $SnCl_2.2H_2O$ in the solution. When concentration decreases, formation of Tin (IV) Oxide is favored. Circles refer to 0.01 moles while squares refer to 0.1 moles of tin precursor is used.

3.3.2 Effects of pH Value

It was remarked by Chen et. al. [96], it is difficult to produce pure Tin (IV) Oxide due to challenges in oxidation of Sn^{2+} ions to Sn^{4+} ions, so that producing phase pure Tin (IV) Oxide was challenging and formation of Tin (II) Oxide side product might be inevitable. When XRD test results are inspected for products, it was seen that for high concentrations of tin ions, at lower pH values phase pure product may be achieved but in a very low yield. For higher pH values, it might be expected that

yield of oxidation product would increase and it is observed for lower concentrations, however, if we increase the concentration of tin ions to produce larger amount of Tin (IV) Oxide, amount and yield of Tin (II) Oxide are increased. As in figure 3.2, percent of Tin (IV) Oxide in the product give its place to Tin (II) Oxide phase may be due to faster formation and growth kinetics with increasing in pH value.

If we look at the XRD test results of Sn21ph80 and Sn22ph76, we would see that, even at higher pH values, with time, Tin (IV) Oxide phase increases its content. This phenomena suggest that increasing in pH slow down Tin (IV) Oxide formation and gives time to Tin (II) Oxide phase to form microsheets. It must be also noted that, all Tin (II) Oxide products showed specific texture on (101) plane, whatever the pH value is.

It must be noted that yield dramatically increases when Tin (II) Oxide phase is dominating. The yields are close to %100. This implies that high yield and purity can be succeeded for Tin (II) Oxide phase at high pH values and high concentrations.

Best results for Tin (II) Oxide phase, which they formed as microsheets, are collected when pH is neutral or basic and only deionized water is used. Increase of pH value, results in thicker and wider sheets. The length of the edges and the thicknesses for SnWaterpH86, SnWaterpH95, SnWaterpH101 are $5\mu m - 0.6\mu m$, $10\mu m - 2.6\mu m$ and $8.7\mu m - 2.2\mu m$, respectively, seen in figure 3.3.

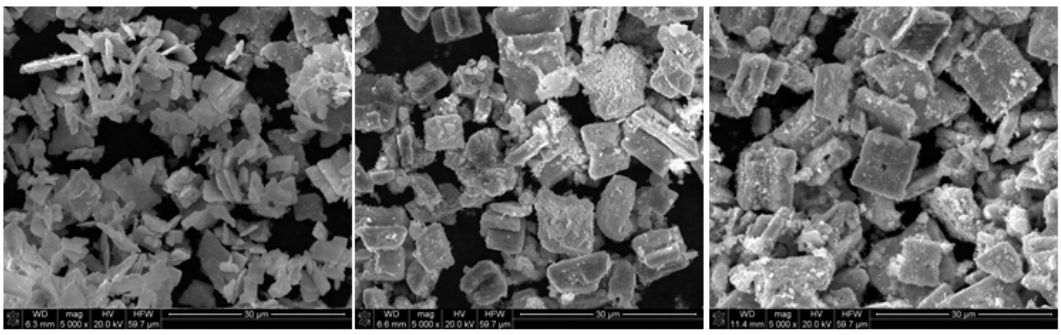


Figure 3.3: Changing thickness of Tin (II) Oxide microsheets with changing pH value. From left to right, specimens are SnWaterpH86, SnWaterpH95 and SnWaterpH101.

As in the figure 3.4, we see that texture and geometry affects XRD diagrams, also.

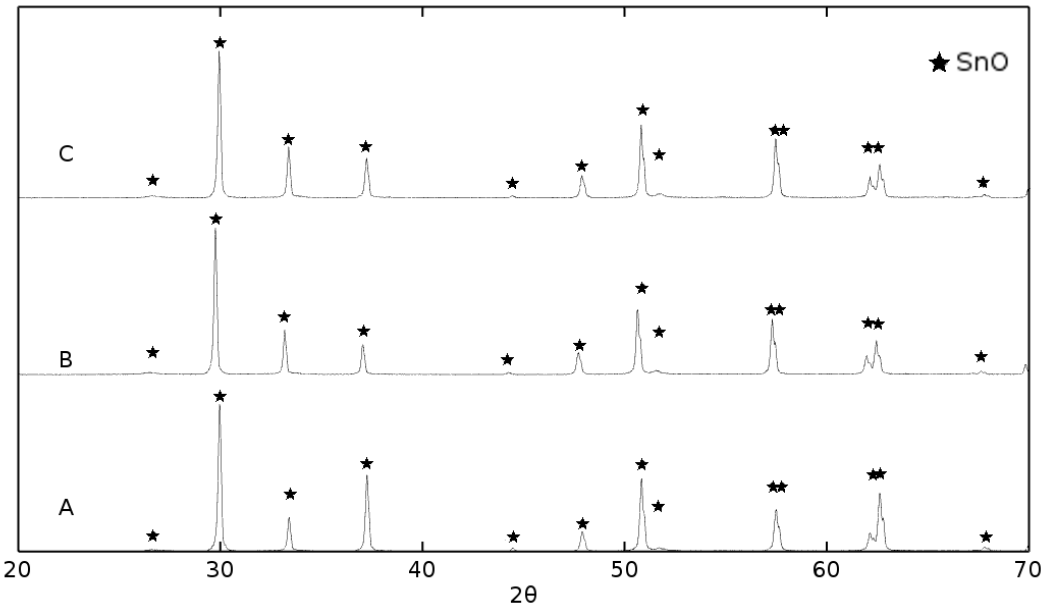


Figure 3.4: Comparison between those three specimens, SnWaterpH86(A), SnWaterpH95(B) and SnWaterpH101(C). Shifting peaks is caused by morphology and texture.

For lower pH values, we see disruption of the microsheets, see figure 3.5. It is seen that Tin (II) Oxide microsheets are disrupted when pH value is high enough to produce Tin (II) Oxide microsheets but lower than the neutral value. Disrupted particles are useful for applications which requires high BET surface.

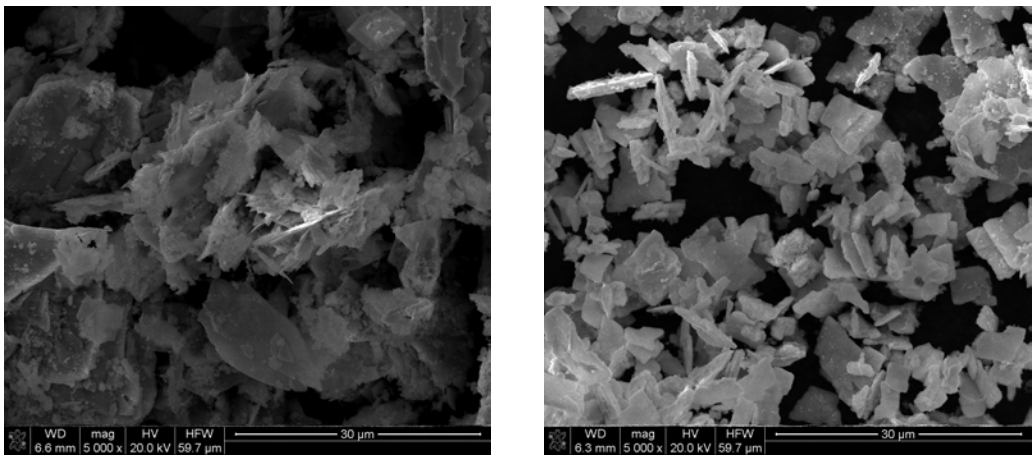


Figure 3.5: Comparison of SEM images between two specimens which they are produced with different pH values. Left: SEM image of SnWaterpH30(pH=3.0), wtr:EtOH=1:0, magnification 5000x. Right: SEM image of SnWaterpH86(pH=8.6), wtr:EtOH=1:0, magnification 5000x.

The effect of starting pH value to the texture is seen dramatically for SnWaterpH30 in the figure 3.7.

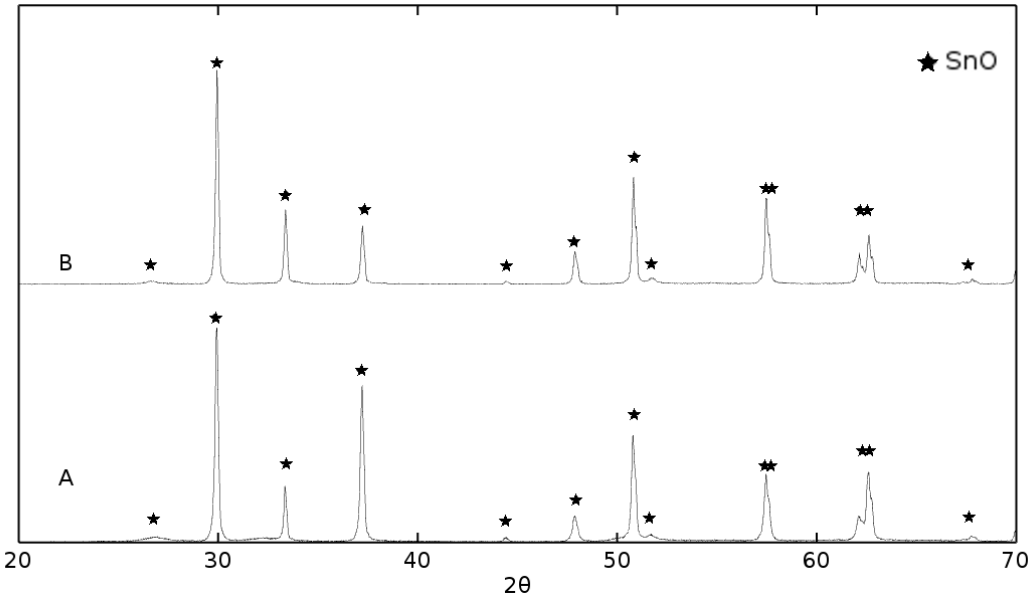


Figure 3.7: Comparison between those three specimens, SnWaterpH30(A) and SnWaterpH101(B). Shifting peaks is caused by morphology and texture.

3.3.3 Effects of Water:Ethanol proportion

Due to corrosive properties of ethanol, adding ethanol to solution may be thought as an important additive. Experiments showed that Water:Ethanol proportion is very effective according to yield, purity of the product, crystallization, aggregation of the particles and the morphology.

When ethanol is present in the system, figure 3.8, ethanol suppress Tin (II) Oxide formation and the product is collected with higher composition and yield of Tin (IV) Oxide phase.

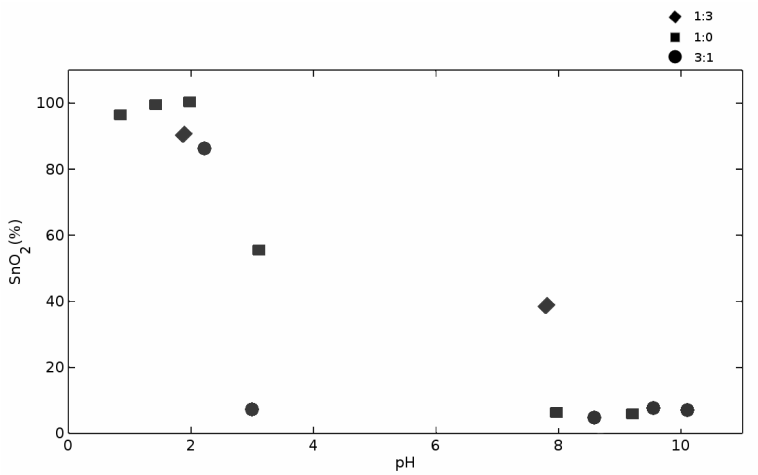


Figure 3.8: Dependence of composition of the phases on water-ethanol proportion of the solution. For all solutions, 0.1 moles $SnCl_2.2H_2O$(the molarity is 71.4mM) is used. Circles for Water:EtOH=1:0, squares for Water:EtOH=3:1 and diamonds for Water:EtOH=1:3.

Secondly it is seen that percentage of Tin (IV) Oxide is increased for high concentrations of tin ions as in the figure 3.8 (Remember that percentage of Tin (IV) Oxide decreases while concentration increases as in the figure 3.2).

However, still phase pure product was not produced at high pH values. The yield was still low, but higher. This higher amount of yield collected as Tin (IV) Oxide, may be due to higher solubility that of in ethanol.

Beside its composition and amount, thirdly, using ethanol cause retardation of crystallization, if we compare SnWaterpH21(pure water as solvent) and SnEtOHph17(pure ethanol as solvent) according to the XRD test results(figure 3.9).

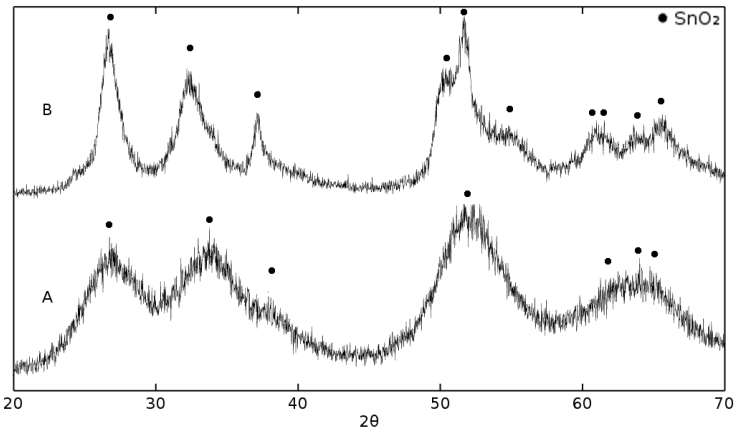


Figure 3.9: In same concentration and pH values are chosen, pure ethanol in SnEtOHph17(A) and pure water SnWaterpH21(B) are used as solvents. As we can see crystallization is at higher degree at SnWaterpH21.

Four of all, according to SEM images in the figure 3.10, aggregation of nanoparticles are smoother when pure ethanol is used.

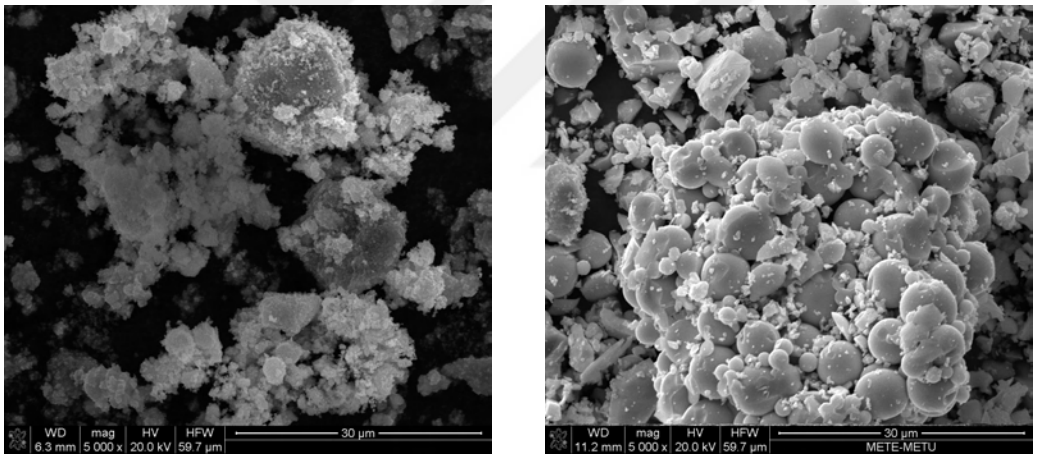


Figure 3.10: Comparison between two specimens which they are produced with different solutions according to their water-ethanol proportion in acidic environment. Left: SEM image of Sn19ph19, wtr:EtOH=3:1, magnification 5000x. Right: SEM image of SnEtOHph17, wtr:EtOH=0:1, magnification 5000x.

Finally, effects of ethanol is similar to lower pH affects on Tin (II) Oxide microsheets, disruption of the rectangular shape as in the figure 3.11. As we can see, Tin (II) Oxide microsheets in Sn21ph80 are disrupted due to ethanol content in the solvent.

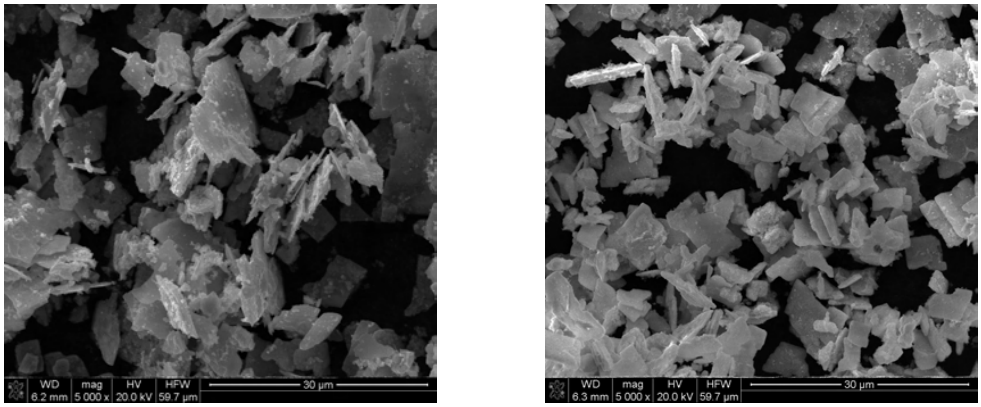


Figure 3.11: Comparison between two specimens which they are produced with different solutions according to their water-ethanol proportion in basic environment. Left: SEM image of Sn21ph80, wtr:EtOH=3:1, magnification 5000x. Right: SEM image of SnWaterpH86, wtr:EtOH=1:0, magnification 5000x.

3.3.4 Effects of Heat Treatment

Heat treatments are conducted at 600 ^{o}C for 2 hours. It was expected Tin (II) Oxide phase transform into Tin (IV) Oxide with a side effect of grain growth. Heat treatments are subjected to the specimens Sn19ph19 produced at low pH value, dominated phase was already Tin (IV) Oxide and specimens produced at neutral and high pH values Sn21ph80 and Sn23ph93 which their dominated phase was Tin (II) Oxide.

The effect of heat treatment on Sn19ph19 was seen as increase in crystallinity of its Tin (IV) Oxide phase, see 3.12. XRD peaks became sharper and intensity was higher.

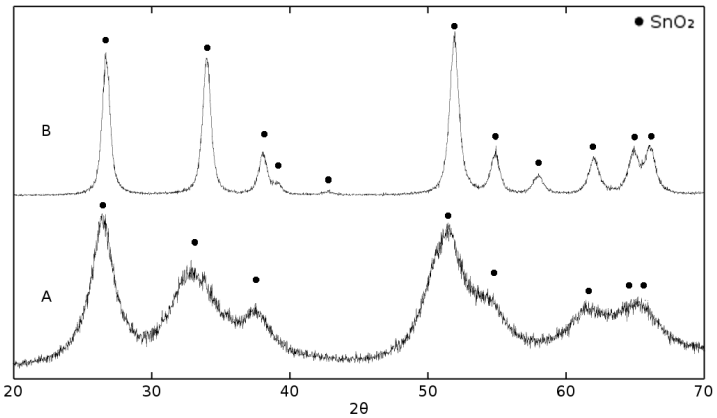


Figure 3.12: XRD diagrams of the specimens Sn19ph19 and heat treated Sn19ph19.

Tin (II) Oxide phase was dominating and the relative amount of Tin (II) Oxide phase was severely decreased after heat treatments, as expected. However, different SnO_2 peaks from other rare SnO_2 structures were observed. Since impurity elements did not exist according to EDS results, it was assumed that, those peaks were belong to high pressured crystal forms of tin and oxygen system, see 3.12. During the transformation process of Tin (II) Oxide to Tin (IV) Oxide from surface to inside, the volume of the particle should have expanded, however, primary shape of the Tin (II) Oxide sheets would not allow the expansion and 2 hours was not enough for the relaxation time of the newly formed structure.

3.3.5 Effects of $K_2S_2O_8$

For the production of the specimens whom codes starts with Sn005 and Sn01, 0.005 moles and 0.01 moles of $SnCl_2.2H_2O$ is used, respectively; for the others, 0.1 moles of $SnCl_2.2H_2O$ is used as in the tables 3.4 and 3.1. If 100% purity and 100% transformation of tin ions to stable Tin (IV) Oxide would be achieved, resulted yields were expected to be $0.75g$, $1.5g$ and $15g$. Even though difference in amount of precursor, is ten or twenty times, yields were very close to each other (except only ethanol is used as solvent SnEtOHph17) considering amount of Tin (IV) Oxide produced excluding Tin (II) Oxide. When only ethanol is used, purity and yield of Tin (IV) Oxide is increased.

Since oxidation of tin ions is problematic, oxidation agent is considered to use. Expected results were high purity and yield with undesired increase in crystalline size. Fortunately, high purity and yield were achieved without increase in crystalline size. Crystalline size was 5nm same as the specimen SnEtOHph17 as calculated from HRTEM images in the figure 3.13.

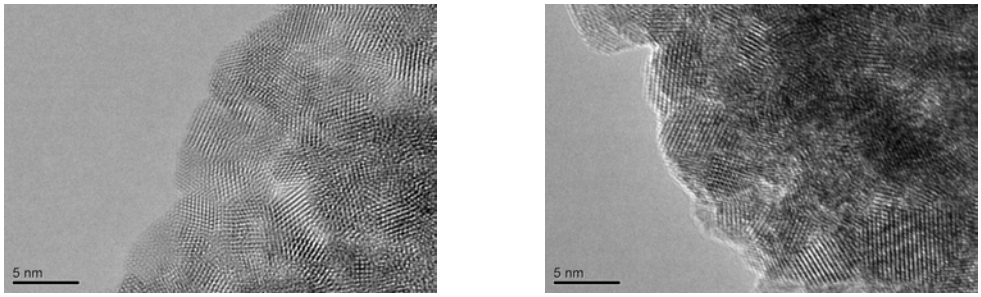


Figure 3.13: HRTEM images of SnEtOHph17(left) and SnK2S2O8EpH09(right). Crystalline sizes are 5nm in diameter.

Generally, HRTEM images of the product must be questioned if it represent the whole. In this case, if we look at the XRD diagrams of the specimens in figure 3.14, broaden peaks show that all products consist of nanocrystalline Tin (IV) Oxide.

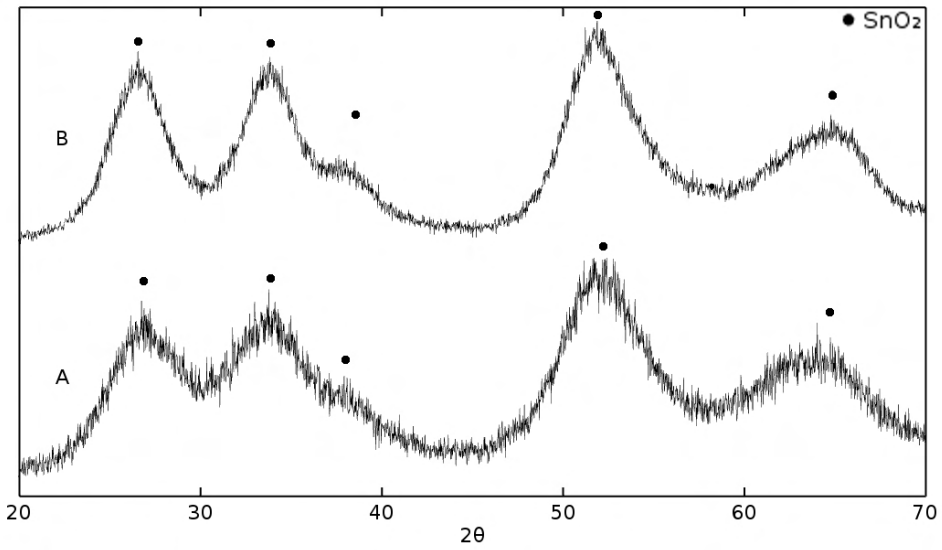


Figure 3.14: XRD diagrams of SnEtOHph17(A) and SnO2K2S2O8E(B).

3.3.6 Effects of Alloying

In the table 3.5, it is seen that lanthanum favors Tin (IV) Oxide formation and increases yield. Close to neutral pH values and even basic values are not enough to produce high purity Tin (II) Oxide phase as it is happened to be for Sn66ph57. XRD test results show that lanthanum does not form any impurity phases. At high pH values Tin (IV) Oxide formed flower-like hierarchical structures. At low pH values agglomerated nanoparticles are formed. Tin (II) Oxide phase was formed as microsheets.

For yttrium, at low pH value, XRD analysis do not show any impure phase, EDS results did not trace yttrium either. However, at high pH values other phases are found. It must be mentioned that the solution contains yttrium(III) nitrate hexahydrate, favor crystallinity of Tin (IV) Oxide at low pH values.

At both low and high pH values, impure phases are found for when we used tungsten.

At both low and high pH values, XRD analysis do not show any impure phase for zirconium. At high pH values, zirconium(IV) oxynitrate hydrate favored Tin (IV) Oxide formation significantly.

3.4 Electrochemical Characterization

3.4.1 Cyclic Voltammetry

SEI formation occurs 0.9V, lithiation occurs during anodic reactions at 0.5V and delithiation occurs at 0.2V during cathodic reactions [117].

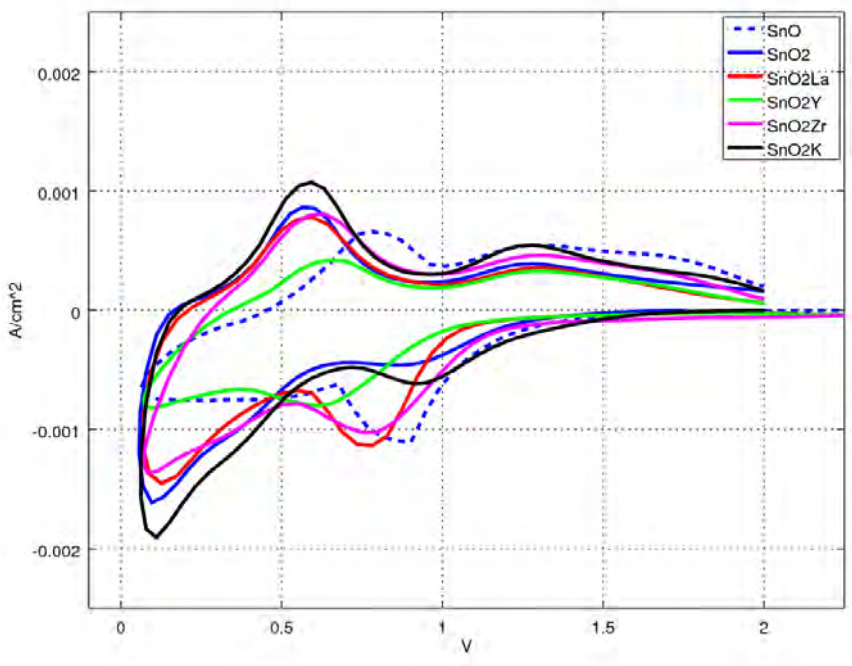


Figure 3.15: CV measurement

In our experiments we introduced different ions to the system, therefore those values are changed.

At cathodic reactions,

1. According to figure 3.15, for SnO SEI formation occured at 0.9V. For SnO2La and SnO2Zr, it is dropped to 0.75V. For SnO2Y, it is dropped further and lost its intensity.
2. From 0.1 to 0.7, for SnO and SnO2Y, plateaus are observed instead lithiation peak. Highest intensities are observed for pure tin(IV) oxides.

At the anodic reactions

1. Delithiation peaks are observed right after 0.5V. For tin(II) oxide, it reaches further to 0.8V.
2. Plateaus are observed from 0.8V to 1.5V.

3.4.2 Charge Capacity and Voltage Profile

Since unit mass tin ratio of SnO is higher than SnO_2, lithium capacity of SnO based materials is higher, initially. Unfortunately, during cycling, their charge capacity decreases rapidly (as in figures 3.16 and 3.17) and gradually dropped to very low values.

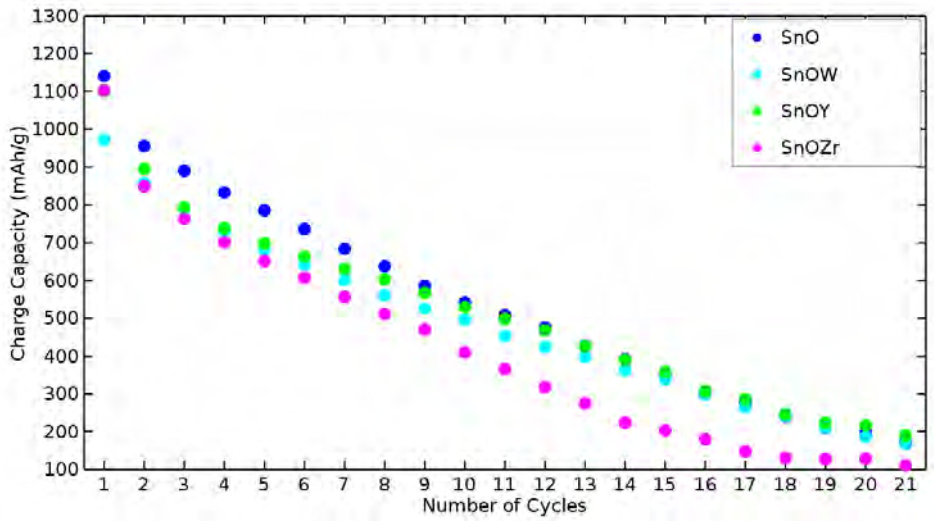


Figure 3.16: Charge densities versus charge-recharge cycles for tin monoxide group.

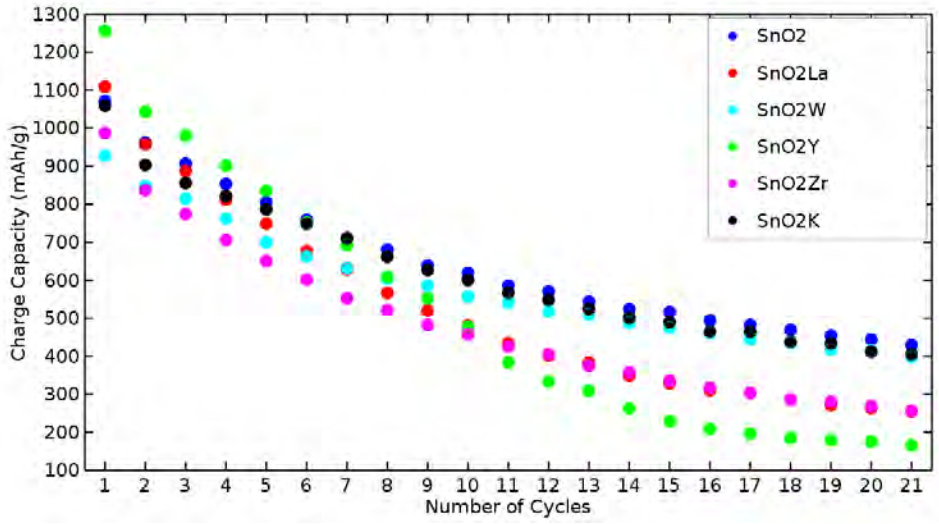


Figure 3.17: Charge densities versus charge-recharge cycles for tin dioxide group.

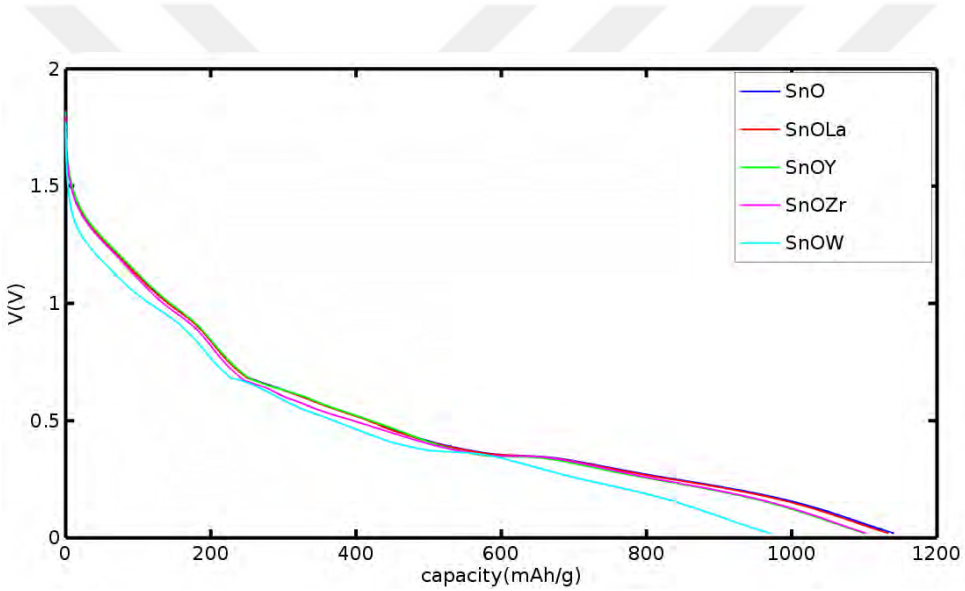


Figure 3.18: Discharge-time profile for alloyed and pure SnO

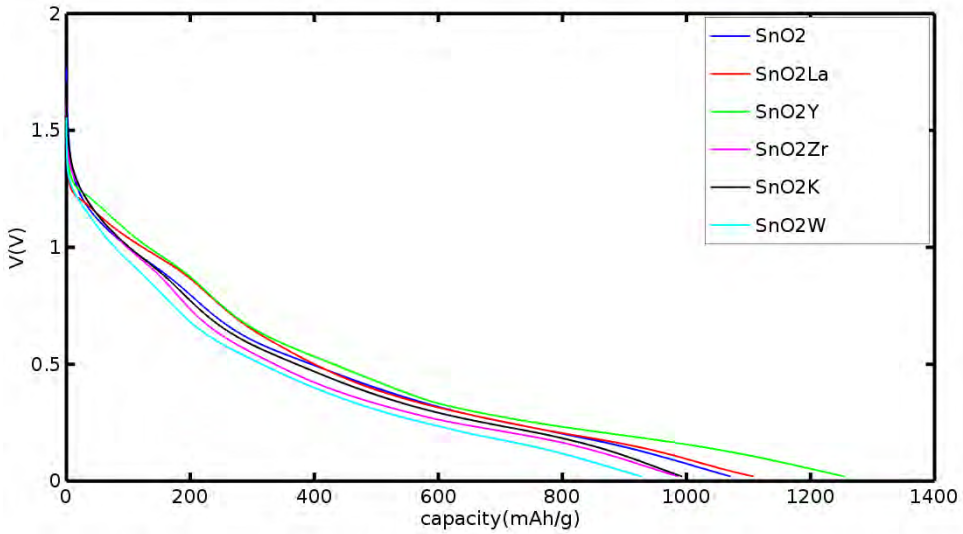


Figure 3.19: Discharge-time profile for alloyed and pure SnO_2

It is clearly seen that alloying tin oxide material with those metals solves neither the pulverization problem nor irreversible reactions problem. However, yttrium addition increased charge capacity for tin dioxide. On the other hand, addition of tungsten decreased the capacity for both phases.

CHAPTER 4

CONCLUSION

Parameters of hydrothermal treatment process temperature, concentration, ethanol content and additional chemicals led these conclusions:

1. For Tin(II) Oxide,
   (a) Ethanol content favor Tin (IV) Oxide formation, also, disrupts Tin (II) Oxide microsheets. Thus, best results for formation of Tin (II) Oxide plates are collected when only water is used.
   (b) High pH or increasing in concentration favors Tin (II) Oxide formation by retarding to transform from Tin (II) Oxide to Tin (IV) Oxide.
2. For Tin(IV) Oxide
   (a) Acidic environment leads to agglomerated Tin (IV) Oxide nanocrystals. With increasing in ethanol content, agglomerated particles are smoother.
   (b) When pure ethanol was used, pure Tin (IV) Oxide powder was produced and yield dramatically increased to 50 percent. Crystalline size of $5\,\mathrm{nm}$ is obtained by two methods.
   (c) Large scale production of nanostructured Tin (IV) Oxide is achieved with $K_2S_2O_8$ oxidation agent.For overall process Tin (IV) Oxide quantum dots with crystalline size of 4-5 nm and 100% yield is produced.
   (d) Time is necessary for formation and fully crystallization of Tin (IV) Oxide product. Time, also, controls morphology of the Tin (IV) Oxide product due to step by step formation of Tin (IV) Oxide hollow microspheres.

(e) After hydrothermal process, heat treatment of the powder may be conducted. During transformation, high pressure structures of Tin (IV) Oxide and Tin (II) Oxide are observed. These may inform us about how transformation is occurred.

Electrochemical testing resulted as,

1. Pure Tin(II) Oxide, SnO-Zr, SnO-Y and SnO-W systems had initial charge density of 1150, 1100, 1100, 990 mAh/g and after 21 cycles, 15, 10, 18 and 20 percent of their capacity was retained, respectively.

2. Pure tin Tin(IV) Oxide, SnO_2-K, SnO_2-Zr, SnO_2-Y, SnO_2-W and SnO_2-La systems had initial charge density of 1090, 1090, 990, 1250, 920, 1110 mAh/g and after 21 cycles, 38, 38, 25, 12, 45, 23 and 20 percent of their capacity was retained, respectively.

REFERENCES

[1] M.Stanley Whittingham, R. Chen, T. Chirayil, and P. Zavalij. The intercalation and hydrothermal chemistry of solid electrodes. *Solid State Ionics*, 94(1):227 – 238, 1997. Papers from the International Workshop.

[2] Jun Song Chen, Lynden A. Archer, and Xiong Wen (David) Lou. Sno2 hollow structures and tio2 nanosheets for lithium-ion batteries. *J. Mater. Chem.*, 21:9912–9924, 2011.

[3] Fabrice M. Courtel and Yaser Abu-Lebdeh. *Tin-Based Anode Materials for Lithium-Ion Batteries*. Springer US, Boston, MA, 2013.

[4] R. W. Francis B. M. L. Rao and H. A. Christopher. Lithium aluminum electrode. *J. Electrochem. Soc*, 124(10):1490 – 1492, 1977.

[5] S.B. Newcomb M.A. Gubbins, V. Casey. Nanostructural characterization of sno2 thin films prepared by reactive r.f. magnetron sputtering of tin. *Thin Solid Films*, 405:270 – 275, 2002.

[6] R. A. Huggins A. Anani, S. C. Baker. Investigation of a ternary lithium alloy mixed-conducting matrix electrode at ambient temperature. *J. Electrochem. Soc*, 135:2103–2106, 1988.

[7] A. Trumbore J. Broadhead, F.J. Disalvo. Solid state electrodes for high energy batteries. *Science*, 205:651–656, 1979.

[8] K. Mizushima et al. Lixcoo2 (0<x<1) a new cathode material for batteries of high energy density. *Mater. Res. Bull*, 15:783–789, 1980.

[9] D.W. Murphy et. al. Vanadium oxide cathode materials for secondary lithium cells. *J. Power Sources*, 126:497–499, 1979.

[10] M. Lazari et. al. A cyclable lithium organic electrolyte cell based on two intercalation electrodes. *J. Power Sources*, 127:773–774, 1980.

[11] H. Tamura et. al. Characterization of the adsorption of co 2+ ,ni 2+ ,zn 2+ and cu 2+ ions on the mno 2 sample. *J. Prog. in Batt. & Batt. Mater*, 9:188–195, 1990.

[12] K.O. Hever. Ion mobility in crystals of a mixed-alkali ferrite, kxna1-xfe7o11. *J. Electrochem. Soc*, 127:826–829, 1968.

[13] C. Saadoune et. al. Electrochemical and physical properties of the lixni1-ycoyo2 phases. *Solid State Ionics*, 370:53–56, 1992.

[14] T. Ohzuku et. al. Synthesis and characterization of lial1/4ni3/4o2(r3m) for lithium-ion (shuttlecock) batteries. *J. Electrochem. Soc*, 142:4033–4039, 1995.

[15] J.D.W. Jones et. al. Structure and electrochemistry of lixcryco1-yo2. *Solid State Ionics*, 68:57–63, 1994.

[16] Y. Gao et. al. Novel lini1–xtix/2mgx/2o2 compounds as cathode materials for safer lithium-ion batteries. *Electrochem. and Sol. Stat. Lett*, 1:117–119, 1998.

[17] M. Thackeray et. al. Spinel electrodes from the li-mn-o system for rechargeable lithium battery applications. *J. Electrochem. Soc*, 139:363–366, 1992.

[18] A.D. Robertson et. al. M3+ modified limn2o4 spinel intercalation cathodes. *J. Electrochem. Soc*, 144:3500–3505, 1997.

[19] J.M. Cocciantelli et. al. Crystal chemistry of electrochemically inserted lixv2o5. *J. Power Sources*, 50:99–402, 1992.

[20] C. Delmas et. al. Lixv2o5 — a new electrode material for rechargeable lithium batteries. *J. Power Sources*, 34:113–118, 1991.

[21] M. Wakihara. *Manganese spinel oxides and vanadium oxides for cathode active materials, the latest technology of the new secondary battery*. CMC, Japan, 1997.

[22] J. Kim et. al. Amorphous manganese oxyiodides exhibiting high lithium intercalation capacity at higher current density. *J. Electrochem. Soc*, 146:55–57, 1999.

[23] A.K. Padhi et. al. Phospho-olivines as positive-electrode materials for rechargeable lithium batteries. *J. Electrochem. Soc*, 144:1188–1194, 1997.

[24] S. Okada et. al. Iron complex cathodes. *Denki Kagaku*, 65:802–808, 1997.

[25] R. Kano et. al. Carbon as negative electrodes in lithium secondary cells. *J. Power Sources*, 26:535–543, 1989.

[26] M. Wakihara. Recent developments in lithium ion batteries. *Mater. Sci. Eng*, 33:109–134, 2001.

[27] S.A. Solin H. Zabel. *Graphite Intercalation Compounds*. Springer-Verlag, Berlin Heidelberg, 1990.

[28] M. Inagaki et. al. Carbon materials structure, texture and intercalation. *Solid State Ionics*, 86:833–836, 1996;.

[29] S. Megahed et. al. Lithium-ion rechargeable batteries. *J. Power Sources*, 51:79–84, 1994.

[30] J.R. Dahn et. al. *Graphite Intercalation Compounds*. Elsevier Science Publications, Amsterdam, 1994.

[31] High-capacity carbons prepared from phenolic resin for anodes of lithium-ion batteries. *J. Electrochem. Soc*, 142:L211–L214, 1995.

[32] C.S. Wang et. al. Lithium insertion in carbon-silicon composite materials produced by mechanical milling. *J. Electrochem. Soc*, 145:2751–2758, 1998.

[33] K. Brandt. Historical development of secondary lithium batteries. *Solid State Ionics*, 69:173–183, 1994.

[34] S. Bruno W.S. Van. *Advances in lithium-ion batteries*. Kluwer Academic/-Plenum, New York, USA, 2002.

[35] E. Peled. The electrochemical behavior of alkali and alkaline earth metals in nonaqueous battery systems—the solid electrolyte interphase model. *J. Electrochem. Soc*, 126:2047–2051, 1979; 126:.

[36] J.B. Bates et. al. Thin-film lithium and lithium-ion batteries. *Solid State Ionics*, 135:33–45, 2000.

[37] B. Di Pietro et. al. On the use of rocking chair configurations for cyclable lithium organic electrolyte batteries. *J. Power Sources*, 8:289–299, 1982.

[38] D. Aurbach et. al. Identification of surface films formed on lithium in propylene carbonate solutions. *J. Electrochem. Soc*, 134:1611–1620, 1987.

[39] D. Guyomard et. al. New amorphous oxides as high capacity negative electrodes for lithium batteries. *J. Power Sources*, 68:692–697, 1997.

[40] Y. Piffard et. al. The amorphous oxides as high capacity negative electrode materials for lithium batteries. *J. Power Sources*, 68:698–703, 1997.

[41] T. Shodai et. al. Anode performance of a new layered nitride. *J. Power Sources*, 68:515–518, 1997.

[42] M. Nishijima et. al. Synthesis and electrochemical studies of a new anode material. *Solid State Ionics*, 83:107–111, 1996.

[43] A.N. Dey et. al. Electrochemical alloying of lithium in organic electrolytes. *J. Electrochem. Soc*, 1971:118, 1547-1549.

[44] J.O. Besenhard. *In progress in intercalation research*. Kluwer Academic/-Plenum, Kluwer, Dordrecht, 1994.

[45] D. Fauteux et. al. Rechargeable lithium battery anodes, alternatives to metallic lithium. *J. Appl. Chem*, 23:1–9, 1993.

[46] et. al. Thin foil lithium-aluminum electrode. the effect of thermal treatment on its electrochemical behavior in nonaqueous media. *J. Power Sources*, 24:71–79, 1988.

[47] R.A. Huggins. *Fast ion transport in solids*. Kluwer Academic/Plenum, Kluwer, Dordrecht, 1993.

[48] H.K. John et. al. Thin film solid electrolyte systems. *Thin Solid Films*, 43:41–92, 1977.

[49] C.N.R. Rao et. al. New strategies for the synthesis of t-selenium nanorods and nanowires. *J. Mater. Chem*, 13:2845–2847, 2003.

[50] P. Wang et. al. A stable quasi-solid-state dye-sensitized solar cell with an amphiphilic ruthenium sensitizer and polymer gel electrolyte. *Natural Materials*, 2:402–407, 2003.

[51] Y.X. Zhang et. al. Hydrothermal synthesis and photoluminescence of tio2 nanowires. *Chem. Phys. Lett*, 365:300–304, 2002.

[52] L. Feng et. al. Red electrophosphorescence devices based on rhenium complexes. *Appl. Phys. Lett*, 83:365–368, 2003.

[53] X. Sun et. al. Cylindrical silver nanowires: preparation, structure, and optical properties. *Chem. - Euro J*, 9:2626–2630, 2005.

[54] R. Marchand et. al. A new form of titanium dioxide and the potassium octatitanate. *Mater. Res. Bull*, 15:1129–1133, 1980.

[55] R. Marchand et. al. Layered k2ti4o9 and the open metastable tio2(b) structure. *Prog. Solid State Ch*, 17:33–52, 1986.

[56] C.K. Chan et. al. High-performance lithium battery anodes using silicon nanowires. *Nature Nanotech*, 3:31–35, 2008.

[57] T.R. Jow et. al. The role of conductive polymers in alkali-metal secondary electrodes. *J. Electrochem. Soc*, 134:1730–1733, 1987.

[58] J.P. Maranchi et. al. Interfacial properties of the a-si/cu: active–inactive thin-film anode system for lithium-ion batteries. *J. Electrochem. Soc*, 153:A1246–A1253, 2006.

[59] O. Shigeki et. al. Li insertion/extraction reaction at a si film evaporated on a ni foil. *J. Power Sources*, 18:591–596, 2003.

[60] K. Uday et. al. Nano- and bulk-silicon-based insertion anodes for lithium-ion secondary cells. *J. Power Sources*, 193:1003–1039, 2007.

[61] K.D. Moni et. al. Silicon and carbon based composite anodes for lithium ion batteries. *J. Power Sources*, 158:557–563, 2006.

[62] W. Liu et. al. Electrochemical characterizations on si and c-coated si particle electrodes for lithium-ion batteries. *J. Electrochem. Soc*, 152:A1719–A1725, 2005.

[63] N. Jagjit et. al. In situ raman microscopy during discharge of a high capacity silicon–carbon composite li-ion battery negative electrode. *Electrochem. Commun.*, 11:235–237, 2009.

[64] K.C. Candace et. al. High capacity li ion battery anodes using ge nanowires. *Nano Lett.*, 8:307–309, 2008.

[65] M. Watanabe et. al. Ionic conductivity of hybrid films based on polyacrylonitrile and their battery application. *J.Appl. Polym. Sci.*, 27:4191–4198, 1983.

[66] I.A. Courtney. The physics and chemistry of metal oxide composites as anode materials for lithium ion batteries. *Philosophy of Doctorate Thesis, Dalhousie University, Canada, 1999*.

[67] M.H. Sinner. Sno2(110) and nano-sno2 characterization by surface analytical techniques. *Philosophy of Doctorate Thesis, Tübingen Universitat, Germany, 2000*.

[68] A. MOL. Chemical vapour deposition of tin oxide thin films. *Philosophy of Doctorate Thesis, Eindhoven University, Germany, 2003.*

[69] F. Yusta et. al. Cvd preparation and characterization of tin dioxide films for electrochemical applications. *J. Mater. Chem.*, 7:1421–1427, 1997.

[70] H.S. Kwok et. al. Pulsed laser deposited crystalline ultrathin indium tin oxide films and their conduction mechanisms. *Thin Solid Films*, 324:299–302, 1998.

[71] A. Souza et. al. Electrical and optical characteristics of sno 2 thin films prepared by dip coating from aqueous colloidal suspensions. *J. Mater. Sci.*, 4:265–270, 1997.

[72] B. Thangaraju. Structural and electrical studies on highly conducting spray deposited fluorine and antimony doped sno2 thin films from sncl2 precursor. *Thin Solid Films*, 411:71–78, 2002.

[73] M. Batzill et. al. The surface and materials science of tin oxide. *Prog.Surf. Sci*, 78:47–54, 2005.

[74] D. Cai et. al. Synthesis and photoluminescence properties of novel sno2 asterisk-like nanostructures. *Mater. Lett.*, 16:1984–1988, 2005.

[75] S. Melvin et. al. Thermodynamics of binary alloys. the lithium—tin system. *J. Phys. Chem*, 70:3042–3045, 1966.

[76] W. John et. al. Thermodynamic study of the lithium-tin system. *J. Electrochem. Soc*, 128:1181–1187., 1981.

[77] I.A: Courtney et. al. Ab initio calculation of the lithium-tin voltage profile. *Phys. Rev. B.*, 58:15583–15588, 1998.

[78] J. Chouvin et. al. Sn mössbauer study of li x sn alloys prepared electrochemically. *Chem. Phys. Lett.*, 308:413–420, 199.

[79] I.A: Courtney et. al. Key factors controlling the reversibility of the reaction of lithium with sno2 and sn2bpo6 glass. *J. Electrochem. Soc*, 144:2943–2948, 1997.

[80] P.J. Santos et. al. Search for suitable matrix for the use of tin-based anodes in lithium ion batteries. *Solid State Ionics*, 135:87–93, 2000.

[81] H. Li et. al. Electrochemical impedance spectroscopy study of sno and nano-sno anodes in lithium rechargeable batteries. *J. Power Sources*, 81-82:340–345., 1999.

[82] J. Chouvin et. al. Sno reduction in lithium cells: study by x-ray absorption. *J. Electroanal. Chem*, 494:136–146, 2000.

[83] T. Ohzuku et. al. Electrochemistry and structural chemistry of linio2 (r3m) for 4 volt secondary lithium cells. *J. Electrochem. Soc*, 140:1862–1870, 1993.

[84] et. al. performances and safety behaviour of rechargeable aa-size li/lix mno2 cell. *J. Power Sources*, 54:143–145, 1995.

[85] D. Aurbach et. al. performances and safety behaviour of rechargeable aa-size li/li x mno 2 cell. *J. Power Sources*, 54:143–145, 1995.

[86] D.E. Fenton et. al. Complexes of alkali metal ions with poly(ethylene oxide) polymer. *Polymer*, 14:589–596, 973.

[87] G.B. Apetecchi et. al. High-performance electrolyte membranes for plastic lithium batteries. *J. Power Sources*, 66:77–82, 1997.

[88] J. Qian, W.A. Henderson, P. Bhattacharya X. Wu, M. Engelhard, O. Borodin, and J. G. Zhang. High rate and stable cycling of lithium metal anode. *Nature Communications*, 6, 2015.

[89] Martin Winter and Jürgen O. Besenhard. Electrochemical lithiation of tin and tin-based intermetallics and composites. *Electrochimica Acta*, 45(1–2):31 – 50, 1999.

[90] Katerina E. Aifantis and Stephen A. Hackney. *Nanoscale Engineering for the Mechanical Integrity of Li-Ion Electrode Materials*, pages 319–347. Wiley-VCH Verlag GmbH & Co. KGaA, 2008.

[91] Shinobu Fujihara, Takahiro Maeda, Hirotoshi Ohgi, Eiji Hosono, Hiroaki Imai, and Sae-Hoon Kim. Hydrothermal routes to prepare nanocrystalline mesoporous sno2 having high thermal stability. *Langmuir*, 20(15):6476–6481, 2004. PMID: 15248739.

[92] Xiao Ming Yin, Cheng Chao Li, Ming Zhang, Quan Yi Hao, Shuang Liu, Li Bao Chen, and Tai Hong Wang. One-step synthesis of hierarchical sno2 hollow nanostructures via self-assembly for high power lithium ion batteries. *The Journal of Physical Chemistry C*, 114(17):8084–8088, 2010.

[93] Zhong Wang, Wenhuai Tian, and Xingguo Li. Synthesis and electrochemistry properties of sn–sb ultrafine particles as anode of lithium-ion batteries. *Journal of Alloys and Compounds*, 439(1–2):350 – 354, 2007.

[94] Md Mokhlesur Rahman, Alexey M. Glushenkov, Thrinathreddy Ramireddy, Tao Tao, and Ying Chen. Enhanced lithium storage in fe2o3-sno2-c nanocomposite anode with a breathable structure. *Nanoscale*, 5:4910–4916, 2013.

[95] X.W. Guo, X.P. Fang, Y. Sun, L.Y. Shen, Z.X. Wang, and L.Q. Chen. Lithium storage in carbon-coated sno2 by conversion reaction. *Journal of Power Sources*, 226:75 – 81, 2013.

[96] Jun Song Chen, Mei Feng Ng, Hao Bin Wu, Lei Zhang, and Xiong Wen (David) Lou. Synthesis of phase-pure sno2 nanosheets with different organized structures and their lithium storage properties. *CrystEngComm*, 14:5133–5136, 2012.

[97] Hongliang Zhu, Deren Yang, Guixia Yu, Hui Zhang, and Kuihong Yao. A simple hydrothermal route for synthesizing sno 2 quantum dots. *Nanotechnology*, 17(9):2386, 2006.

[98] Shuisheng Wu, Huaqiang Cao, Shuangfeng Yin, Xiangwen Liu, and Xinrong Zhang. Amino acid-assisted hydrothermal synthesis and photocatalysis of sno2 nanocrystals. *The Journal of Physical Chemistry C*, 113(41):17893–17898, 2009.

[99] Weiping Shao, Zhenghua Wang, Yuanguang Zhang, Jianhua Cui, Weichao Yu, and Yitai Qian. Controlled synthesis of sno2 hollow microspheres via a facile template-free hydrothermal route. *Chemistry Letters*, 34(4):556–557, 2005.

[100] Xiao Ming Yin, Cheng Chao Li, Ming Zhang, Quan Yi Hao, Shuang Liu, Li Bao Chen, and Tai Hong Wang. One-step synthesis of hierarchical sno2 hollow nanostructures via self-assembly for high power lithium ion batteries. *The Journal of Physical Chemistry C*, 114(17):8084–8088, 2010.

[101] Lifen Xiao, Jianping Li, Qiao Li, and Lizhi Zhang. One-pot template-free synthesis, formation mechanism, and lithium ions storage property of hollow sno2 microspheres. *Journal of Solid State Electrochemistry*, 14(6):931–936, 2010.

[102] X.W. Lou, Y. Wang, C. Yuan, J.Y. Lee, and L.A. Archer. Template-free synthesis of sno2 hollow nanostructures with high lithium storage capacity. *Advanced Materials*, 18(17):2325–2329, 2006.

[103] Jianmin Ma, Jun Zhang, Shurong Wang, Qinghong Wang, Lifang Jiao, Jiaqin Yang, Xiaochuan Duan, Zhifang Liu, Jiabiao Lian, and Wenjun Zheng. Superior gas-sensing and lithium-storage performance sno2 nanocrystals synthesized by hydrothermal method. *CrystEngComm*, 13:6077–6081, 2011.

[104] Kirsten M. Ø. Jensen, Mogens Christensen, Pavol Juhas, Christoffer Tyrsted, Espen D. Bøjesen, Nina Lock, Simon J. L. Billinge, and Bo B. Iversen. Revealing the mechanisms behind sno2 nanoparticle formation and growth during hydrothermal synthesis: An in situ total scattering study. *Journal of the American Chemical Society*, 134(15):6785–6792, 2012. PMID: 22420861.

[105] H.T. Chen, X.L. Wu, Y.Y. Zhang, J. Zhu, Y.C. Cheng, and PaulK. Chu. A novel hydrothermal route to synthesize solid sno2 nanospheres and their photoluminescence property. *Applied Physics A*, 97(3):581–585, 2009.

[106] Deliang Chen and Lian Gao. Novel synthesis of well-dispersed crystalline sno2 nanoparticles by water-in-oil microemulsion-assisted hydrothermal process. *Journal of Colloid and Interface Science*, 279(1):137 – 142, 2004.

[107] Peng Sun, Wan Zhao, Yang Cao, Yue Guan, Yanfeng Sun, and Geyu Lu. Porous sno2 hierarchical nanosheets: hydrothermal preparation, growth mechanism, and gas sensing properties. *CrystEngComm*, 13:3718–3724, 2011.

[108] Kazuyoshi Sato, Yohei Yokoyama, Jean-Christophe Valmalette, Kazuo Kuruma, Hiroya Abe, and Takayuki Takarada. Hydrothermal growth of tailored sno2 nanocrystals. *Crystal Growth & Design*, 13(4):1685–1693, 2013.

[109] Eduardo J.H. Lee, Caue Ribeiro, Elson Longo, and Edson R. Leite. Growth kinetics of tin oxide nanocrystals in colloidal suspensions under hydrothermal conditions. *Chemical Physics*, 328(1–3):229 – 235, 2006.

[110] Benkhaouda Soufyane, Sher Zaman, and Xin JianGuo. Nanostructures sno and sno2 low density targets for laser produced plasma euv source. *Photonics and Optoelectronics*, 2:14–118, 2013.

[111] Luming Zhu, Hong Yang, Dalai Jin, and Hongliang Zhu. Hydrothermal synthesis of sno nanoflakes as anode materials for lithium-ion batteries. *Inorganic Materials*, 43(12):1307–1312, 2007.

[112] Quang Trung Khuc, Xuan Hien Vu, Duc Vuong Dang, and Duc Chien Nguyen. The influence of hydrothermal temperature on sno 2 nanorod formation. *Advances in Natural Sciences: Nanoscience and Nanotechnology*, 1(2):025010, 2010.

[113] Lipeng Qin, Jiaqiang Xu, Xiaowen Dong, Qingyi Pan, Zhixuan Cheng, Qun Xiang, and Feng Li. The template-free synthesis of square-shaped sno 2 nanowires: the temperature effect and acetone gas sensors. *Nanotechnology*, 19(18):185705, 2008.

[114] Alexander Birkel, Niklas Loges, Enrico Mugnaioli, Robert Branscheid, Dominik Koll, Stefan Frank, Martin Panthöfer, and Wolfgang Tremel. Interaction of alkaline metal cations with oxidic surfaces: Effect on the morphology of sno2 nanoparticles. *Langmuir*, 26(5):3590–3595, 2010. PMID: 20020761.

[115] Hua Wang, Qingqin Liang, Weijie Wang, Yiran An, Jinghong Li, and Lin Guo. Preparation of flower-like sno2 nanostructures and their applications in gas-sensing and lithium storage. *Crystal Growth & Design*, 11(7):2942–2947, 2011.

[116] Gao feng FU, Jing WANG, Bing XU, Hong GAO, Xiu lin XU, and Hao CHENG. Influence of hydrothermal temperature on structure and microstructure of boehmite. *Transactions of Nonferrous Metals Society of China*, 20, Supplement 1:s221 – s225, 2010.

[117] H. Song, X. Li, Y. Cui, D. Xiong, Y. Wang, J. Zeng, L. Dong, D. Li, and X Sun. Controllable lithium storage performance of tin oxde anodes with various particle sizes. *International Journal of Hydrogen Energy*, XXX(1-8), 2015.